DEVELOPMENT OF DIFFERENT CARBON SUPPORTS FOR PROTON EXCHANGE MEMBRANE FUEL CELL ELECTROCATALYSTS

A THESIS SUBMITTED TO
THE GRADUATE SCHOOL OF NATURAL AND APPLIED SCIENCES
OF
MIDDLE EAST TECHNICAL UNIVERSITY

BY

BURCU GÜVENATAM

IN PARTIAL FULFILLMENTS OF THE REQUIREMENTS
FOR
THE DEGREE OF MASTER OF SCIENCE
IN
CHEMICAL ENGINEERING

SEPTEMBER 2010

Approval of the thesis

DEVELOPMENT OF DIFFERENT CARBON SUPPORTS FOR PROTON EXCHANGE MEMBRANE FUEL CELL ELECTROCATALYSTS

submitted by **BURCU GÜVENATAM** in partial fulfillment of the requirements for the degree of **Master of Science in Chemical Engineering Department, Middle East Technical University by,**

Prof. Dr. Canan Özgen
Dean, Graduate School of **Natural and Applied Sciences** _____

Prof. Dr. Gürkan Karakaş
Head of Department, **Chemical Engineering Dept, METU** _____

Prof. Dr. İnci Eroğlu
Supervisor, **Chemical Engineering Dept., METU** _____

Dr. Ayşe Bayrakçeken
Co-supervisor, **Chemical Engineering Dept., Atatürk University**_____

Examining Committee Members:

Prof. Dr. Işık Önal
Chemical Engineering Dept., METU _____

Prof. Dr. İnci Eroğlu
Chemical Engineering Dept., METU _____

Prof. Dr. Gülsün Gökağaç
Chemistry Dept., METU _____

Assistant Prof. Dr. Serkan Kıncal
Chemical Engineering Dept., METU _____

Dr. Ayşe Bayrakçeken
Chemical Engineering Dept., Atatürk University _____

Date: 13.09.2010

I hereby declare that all information in this document has been obtained and presented in accordance with academic rules and ethical conduct. I also declare that, as required by these rules and conduct, I have fully cited and referenced all material and results that are not original to this work.

Name, Last name : BURCU GÜVENATAM

Signature :

ABSTRACT

DEVELOPMENT OF DIFFERENT CARBON SUPPORTS FOR PROTON EXCHANGE MEMBRANE FUEL CELL ELECTROCATALYSTS

Güvenatam, Burcu
M.Sc., Department of Chemical Engineering
Supervisor: Prof. Dr. İnci Eroğlu
Co-Supervisor: Dr. Ayşe Bayrakçeken
September 2010, 96 pages

Proton exchange membrane (PEM) fuel cell technology is promissing alternative solution to today's energy concerns providing clean environment and efficient system. Decreasing platinum (Pt) content of fuel cell is one of the main goals to reduce high costs of fuel cell technology in the way of commercialization. In this target, porous carbons provide an alternative solution as a support material for fuel cell electrocatalysts. It is also essential to increase surface area of carbon support material to have well dispersion of the Pt nanoparticles. The aim of this thesis is to synthesize mesoporous carbon supports named as hollow core mesoporous shell (HCMS) carbon and prepare their corresponding electrocatalysts with platinum impregnation method.

HCMS carbon supports were synthesized by using two different carbon sources. As a first approach, phenol/paraformaldehyde couples were used and carbon source exhibited 1053 m^2/g BET surface area and 1.046 nm BJH adsorption pore diameter. Second approach was to use divinylbenzene (DVB) as a carbon source with an initiator named as azo bis isobuytronitrile (AIBN) differing synthesis criteria. It is observed that using AIBN/DVB, pore sizes increased up to 3.44 nm.

Platinum impregnation was conducted by microwave irradiation method using hydrogen hexachloroplatinate (IV) hydrate as a platinum precursor. The first achievement was to increase platinum loading up to 44 wt % on commercial Vulcan XC 72 by using ethylene glycol as a reducing agent. Using different reducing agents such as hydrazine, sodium borohydrate with a combination of ethylene glycol, platinum loading reached up to 34 wt % on HCMS carbon support. Accordingly, 34 wt %, 32 wt % and 28 wt % Pt/HCMS carbon supported electrodes preparation was achieved. The sizes of the platinum nanoparticles were calculated by XRD analysis as 4 nm, 4.2 nm and 4.5 nm for 28 wt %, 32 wt % and 34 wt % Pt/HCMS carbon supported electrodes respectively. Characterizations of catalysts were performed by ex situ (N_2 adsorption, TGA, SEM, TEM and Cyclic Voltammetry) and in situ (PEMFC tests) analysis.

Keywords: HCMS carbon support, platinum, fuel cell electrocatalyst

ÖZ

PROTON DEĞİŞİM MEMBRANLI YAKIT PİLİ ELEKTROKATALİZÖRÜ İÇİN DEĞİŞİK KARBON DESTEK MALZEMELERİNİN GELİŞTİRİLMESİ

Güvenatam, Burcu
Yüksek Lisans, Kimya Mühendisliği Bölümü
Tez Yöneticisi: Prof. Dr. İnci Eroğlu
Ortak Tez Yöneticisi: Dr. Ayşe Bayrakçeken
Eylül 2010, 96 sayfa

Proton Değişim Zarlı (PEM) yakıt pili teknolojisi, temiz çevre ve verimli bir sistem sunmasıyla bugünün enerji kaygılarına gelecek vaat eden bir alternatif çözüm sunmaktadır. Yakıt pilinde kullanılan platin (Pt) miktarının azaltılması ticarileşme yolunda gerekli olan yüksek maliyetlerin düşürülmesinde gerekli görülen temel öğelerden biridir. Bu amaçla, gözenekli karbon yapıları yakıt pili elektrokatalizörleri için destek malzemesi olarak alternatif bir çözüm getirmektedir. Aynı zamanda, platin nano parçacıklarının düzenli dağılımını elde etmek için karbon destek malzemesine yüklenen platinin ağırlıkça yüzdesinin arttırılması da gereklidir. Bu tezin amacı da, mezo gözenekli karbon desteği sentezlenmesi ve bunların elektrokatalizörlerinin platin ekleme yöntemi ile hazırlanmasıdır.

Bu nedenle, HCMS karbon olarak anılan içi boşluklu mezo gözenek kabuklu karbon desteği, iki değişik karbon kaynağı kullanılarak sentezlenmiştir. İlk yaklaşımda, fenol/paraformaldehit çifti karbon kaynağı olarak kullanılmış ve elde edilen karbonun BET yüzey alanının 1053 m^2/g ve BJH adsorpsiyon gözenek çapının 1.046 nm olduğu gözlemlenmiştir.

İkinci yaklaşımda da, azo izo butironitril öncü olarak, divinilbenzen de karbon kaynağı olarak kullanılmış ve karbon desteğinin gözenek çapı 3.4 nm'ye kadar çıkartılabilinmiştir.

Platinin yapıya eklenmesi, hidrojen hekzakloroplatin (IV) hidrat kimyasalı platin öncü maddesi olarak kullanılarak mikrodalga ısıtma yöntemi ile yapılmıştır. İlk başarı, ticari karbon desteği olan Vulcan XC 72'ye etilen glikol kullanılarak kütlece % 44'lük platin yüklenmesidir. Etilen glikole ek olarak kullanılan hidrazin, sodyum borhidrat ile de HCMS karbon desteğinde % 34'lük yüklemeye kadar çıkılabilinmiştir. Dolayısıyla, kütlece % 34, % 31 ve % 28'lik Pt/HCMS elektrodları hazırlanmıştır. Hazırlanan elektrodların platin nanoparçacık boyutları % 28'lik Pt/HCMS için 4 nm, % 32'lik Pt/HCMS için 4.2 nm ve % 34'lük Pt/HCMS için 4.5 nm olarak XRD analiz sonuçlarına göre hesaplanmıştır. Katalizörlerin karakterizasyonları da eks situ (N_2 adsorplanması, BET yüzey alanı, TGA, SEM, TEM, döngüsel voltametri) ve in situ (PEM yakıt pili testi) analizleri doğrultusunda incelenmiştir.

Anahtar Kelimeler: HCMS karbon desteği, platin, yakıt pili elektrokatalizörü

To my father

And

My family

ACKNOWLEDGEMENT

I would like to express my sincere gratitude to my supervisor Prof. Dr. İnci Eroğlu for her guidance, criticism, encouragements and also sharing her immense knowledge with me throughout the research. Also, I'm grateful for her support in completing my study.

Also, I would like to express my greatest appreciation to my co-supervisor Dr. Ayşe Bayrakçeken for her guidance, helpful discussions in fuel cell electrochemistry and also suggestions and encouragements in every stage of my thesis study even in my hard times.

My special thanks go to my lab mate Berker Fıçıcılar who helped to develop all my abilities on laboratory work, provided very strong discussion points with his engineering approaches and guided in solving the unexpected problems. Also, I'm grateful for his encouragements even in my hard times.

Appreciations also go to Serdar Erkan, Dilek Ergün, and all fuel cell research group members for their contributions to my study and also their kind cooperation in the lab.

Especially, I have dedicated my M.Sc. thesis to my father who is the reason of all my efforts to complete my study absolutely. I'm grateful to my father for his endless support and guidance up to now. Also, I am indebted to my mother and my brother for their extraordinary support, help, motivation and being with me all the time.

This study was supported by The Scientific and Research Council of Turkey (TÜBİTAK) as a research project with number of 109M221 and title of 'Pem Yakıt

Pilleri için Kompozit Membranlar ve Elektrokatalizörlerin Geliştirilmesi ve Uzun Dönem Performanslarının Belirlenmesi' and METU BAP-03-04-2009-06 project with a title of 'PEM Yakıt Pili Elektrokatalizörleri İçin Farklı Karbon Destekleri Geliştirilmesi'. Also, I would like to thank for the scholarship of TÜBİTAK project.

Finally, I would like to thank Dr. Kemal Behlülgil from METU Central Laboratory for his disciplined studies on particle and surface characterization analysis.

TABLE OF CONTENTS

LIST OF TABLES

TABLES

LIST OF FIGURES

FIGURES

LIST OF SYMBOLS

AIBN : Azobis isobutyronitrile

AFC : Alkaline fuel cell

C18TMS : Octadecyltrimetoxysilane

CE : Counter electrode

CV : Cyclic voltammetry

DI : Deionize water

DVB : Divinylbenzene

FCC : Face cubic centered

GC : Glassy carbon

GDL : Gas diffusion layer

HCMS : Hollow core mesoporous shell

HF : Hydrofluoric acid

HOR : Hydrogen oxidation reaction

IUPAC : International Union of Pure and Applied Chemistry

MCFC : Molten carbonate fuel cell

MEA : Membrane electrode assembly

OCV : Open current voltage

ORR : Oxygen reduction reaction

PAFC : Phosphoric acid fuel cell

PEM : Proton exchange membrane

PEMFC : Proton exchange membrane fuel cell

Pt : Platinum

R&D : Research & Development

RE : Reference electrode

RH : Relative humidity

SCMS : Solid Core mesoporous shell

SEM : Scanning electron microscopy

SOFC : Solid oxide fuel cell

TEM : Transmission electron microscopy

TEOS : Tetraethyl orthosilicate

TGA : Thermal gravimetric analysis

VC : Vulcan XC 72

XPS : X-ray photoemission spectroscopy

XRD : X-ray diffraction

WE : Working electrode

d : lattice spacing

E_a^0 : The standart anode potential (Volt)

E_c^0 : The standart cathode potential (Volt)

$E_{overall}^0$: The standart overall potential (Volt)

EASA : Electrochemically active surface area (m^2/g)

i^0 : Exchange current density (Acm^{-2})

$\mathcal{L}$: Avogadro constant

n : order of the reflection

n_m: BET monolayer capacity ($\mu mol\ g^{-1}$)

$\mathcal{P}$: Equilibrium pressure (bar)

$\mathcal{P}_0$: Saturated vapor pressure (bar)

$\mathcal{T}$: Temperature (Kelvin)

$\mathcal{V}$: Total volume (cm^3)

$\mathcal{V}_m$; volume of gas molecules corresponding to the monolayer (cm^3)

$\mathcal{w}$: Weight (gram)

σ : Average area occupied by each molecule in the completed monolayer (nm^2)

λ : wavelenght of the X-rays

α : half-value of the diffraction angle

CHAPTER 1

INTRODUCTION

Energy is a main demand of human beings since ancient times. Since energy sources were limited for most of the places on the earth, human beings began to look for it and even fought hard with each other for long periods. Today, this contest is continuing already. The idea at the back of development of a typical fuel cell system is to find an alternative solution for these energy needs. Thus, hydrogen energy and fuel cell technology may be thought of as a choice against petroleum-rich countries. Thinking about the fast running out of fossil energy sources in view of sharp increase in the human's energy consumption, scientist concentrated their R&D studies on hydrogen energy usage in defense industry and in private sector. If petroleum reserves and its consumption data can be analyzed deeply, it will be clearly understood that world is in the energy transition period. Figure 1.1 shows that transitions of each energy sources in the relation with technological revolutions.

Figure 1.2 explains these transition periods in a chronological pattern. Industrial revolution began in 1800s and wood was the first primary energy source from the 18th to the 19th century. Then, it started to share primary energy consumption with coal when electricity revolution occurred with Thomas Edison invention of electric lighting in 1880. In 1965, energy transition was occurred and petroleum era began with automobile revolution. Today, natural gas era is beginning which results in a decrease of the petroleum portion and significant increase in natural gas consumption.

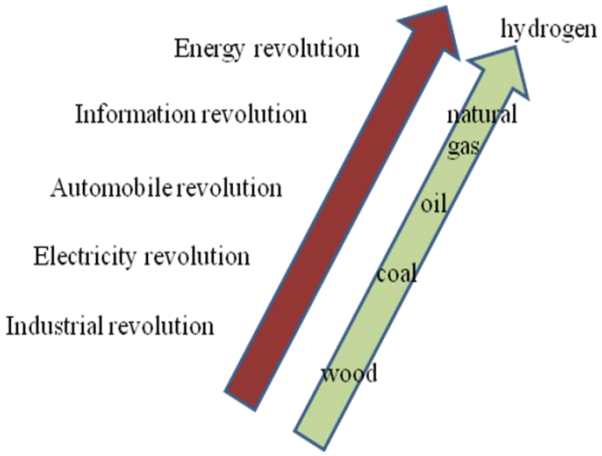

Figure 1.1 Relationship between history of technological revolution and history of fuels

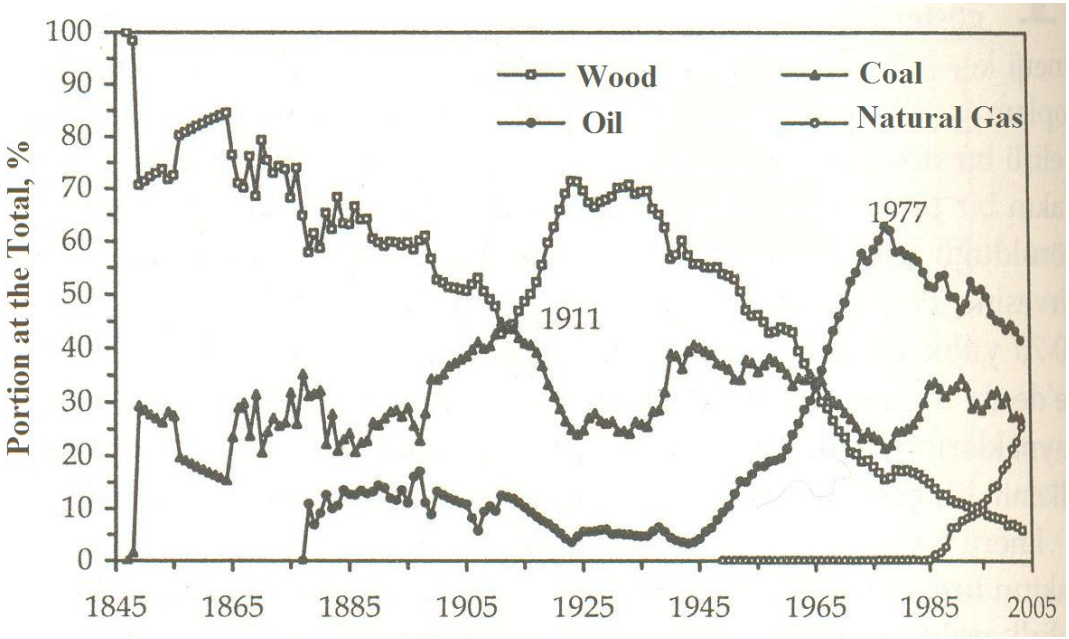

Figure 1.2 Portions of the main fuels at the total energy consumptions in the years (Ediger, 2003)

Placement between the energy sources is predicated on the dynamic of development from carbon rich to hydrogen rich sources (Ediger, 2003). In fact, the

ratio of C:H is 10:1 for wood, 1:1 for coal, 1:2 for petroleum, and 1:4 for natural gas as seen from Figure 1.3. It is appropriate to point out that future energy source will be hydrogen which is carbon free source. Especially, transition from solid fuel to liquid fuel and then to gaseous fuel bring technological development in terms of economics, practice and environmental compatibility. Turkey delayed 72 years for coal production and 89 years for petroleum production. However, hydrogen energy and fuel cell technology studies have being conducted in a conjunction with many researchers, institutions, defense industry and private sector in Turkey today.

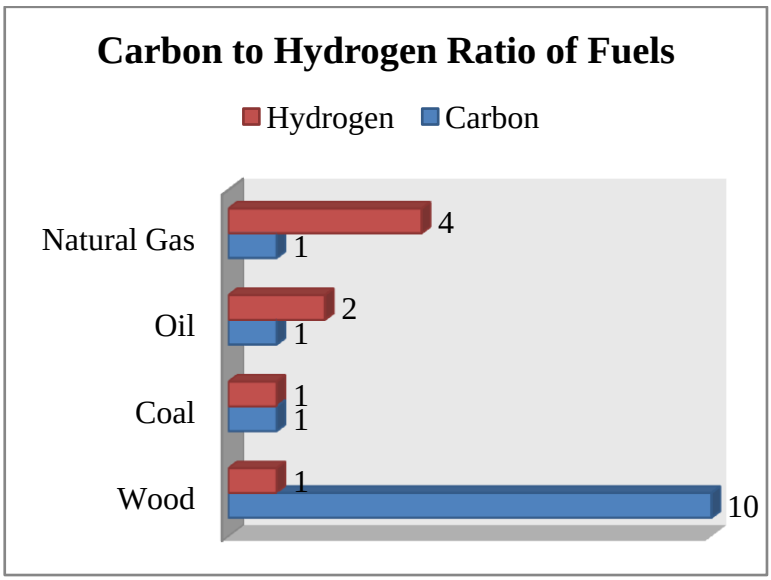

Figure 1.3 Carbon to Hydrogen ratio of fuel types

Hydrogen as a primary energy source provides some advantages. First of all, hydrogen is an excellent energy carrier being the lightest and simplest element in the universe. Also, it is the most abundant of the chemical elements with constituting 75% of the universe's elemental mass. Marban et al. (2006) emphasized that the amount of energy produced during hydrogen combustion process (with a low heating value on mass basis) is 2.4, 2.8 and 4 times higher than that of methane, gasoline and

coal respectively. It is also stated that current annual hydrogen production is about 0.1 Gton, 98% of which comes from the reforming of fossil fuels today.

Fuel cell technology presents a solution to today's energy demand with an important advantage of bringing carbon-free technology which results in a clean environment with low or zero emission. In fact, fuel cell technology does not rely on combustion engine principle; it supplies high conversion efficiency through the system with high energy density of hydrogen by weight. On the other hand, fuel cell technology is faced with some disadvantages in terms of high costs which come from expensive components of fuel cell system, requirement of hydrogen production from other feedstocks. Thus, R&D studies are focusing on solving those disadvantages to have more compatible designs and adaptable systems on daily life of human beings.

Fuel cell technology reached to variety of types according to their application areas. Each of them has different characteristics and worldwide developers. They are classified upon the electrolyte used in the membrane part which determines the operating temperature of the cells. Main fuel cell types are proton exchange membrane fuel cells (PEMFC), phosphoric acid fuel cells (PAFC), alkaline fuel cells (AFC), molten carbonate fuel cells (MCFC), and solid oxide fuel cells (SOFC).

Table 1.1 summarizes the differences of the each fuel cell types and their advantages and disadvantages (Bernay et al., 2002, Haile et al., 2003). PEMFC is the most commonly adapted type to today's daily systems and technologies and widely commercially available type due to its simplicity, viability and quick start-up features. To date, PEMFC technology has been demonstrated in variety of application such as automobiles, scooters, golf carts, portable power, boats, airplanes, space shuttles, locomotives etc. (Barbir, 2005).

Table 1.1 Different Types of Fuel Cell Technologies and their main characteristics

Name	Symbol	Electrode	Fuel	Mobile Ion
Proton Exchange Membrane Fuel Cell	PEMFC	Proton Exchange Membrane (e.g. Nafion)	Hydrogen, Methanol	$(H_2O)_nH^+$
Phosphoric Acid Fuel Cell	PAFC	Pure phosphoric acid	Hydrogen	H^+
Alkaline Fuel Cell	AFC	Potash KOH generally in aqueous solution at 35% in weight	Hydrogen	OH^-
Molten Carbonate Fuel Cell	MCFC	Old Generation Li_2-CO_3/K_2CO_3, new generation Li_2-CO_3/Na_2CO_3	Hydrogen, hydrocarbons and CO	CO_3^{2-}
Solid Oxide Fuel Cell	SOFC	Yttrium oxide-doped zirconia	Hydrogen, hydrocarbons and CO	O^{2-}

PEMFC electrolyte is a polymeric membrane named as proton exchange membrane. Solid Oxide fuel Cell (SOFC) has a ceramic membrane. Other types of fuel cells use solutions as electrolyte. However, Barney et al (2002) states that solid electrolytes allow to manage start-ups and shot downs. In addition, electrolyte thickness is reduced by the solid materials and this leads to increase the cell performance. Thus; handling, assembly or tightness are less complex issues for PEMFCs. Also, the electrolyte of PEMFC does not include any acidic or basic mediums which provide non-corrosive electrolyte and much safe operation (Andujar et al, 2009).

PEMFCs have some additional particular properties than other fuel cell types. The operating temperature is relatively low which causes to reduce thermal losses from the cell and the start-up and shot down procedures are faster than in high

temperature fuel cell (Andujar et al, 2009). They have also smaller volume and lighter weight which make PEMFCs preferable for portable applications (Barbir, 2005). PEMFCs have CO_2 tolerance which brings on an opportunity of supplying atmospheric air to the system. They exhibit a good tolerance to the pressure differences of the reactant gases. The system is also compact, robust and includes stable building materials with simple mechanical design. (Andujar et al, 2009). Veziroglu (2005) states that about 90% of the R&D works of fuel cell technology are based on PEM fuel cell type due to these significant advantages (Barbir, 2005).

The main disadvantage of a typical fuel cell is the humidification requirement of reactive gases to reach sufficient conductivity. When the water is used in humidifying unit, fuel cell system should be operated below the boiling point of water. Also, low temperature fuel cell applications need noble platinum or platinum based alloys as catalysts for hydrogen oxidation and oxygen reduction reactions. For high temperature operations, non-noble catalysts can be used. Also, platinum usage brings high costs for fuel cell technology. Thus, R&D studies for the last decade targeted a reduction in platinum loading for PAFC and PEMFCs. Up to now, platinum loading in PEM fuel cell electrocatalysts is reduced to 0.4 mg/cm^2 from 2.0 mg/cm^2 without any performance losses. It is aimed to reduce it up to 0.1 mg/cm^2 (Barbir, 2005).

The system costs and total efficiencies of the fuel cell systems are crucial parameters also to commercialize and adapt them to daily applications. As seen from the Table 1.2 (Spakovsky et al, 2007), SOFC have the highest efficiency due to high temperature operations. The disadvantages of SOFC are that it is all made up of ceramic materials which are brittle and have high cost to manufacture and also it has lower power density comparing with PEMFCs. Thus, R&D studies focus on to develop membranes to replace Nafion membrane which will be suitable to operate in high temperatures for PEMFC and manufacture costs will be low. As seen from Table 1.3, AFC has lower manufacturing costs than other fuel cell types due to its basic construction materials and techniques. Also, Table 1.2 shows that AFC system gives greater reaction kinetics where its electrical efficiency can reach up to 60 %,

and leads higher cell voltages where power density rises up to 8 kW/m^2. Unfortunately, AFC is far from the commercialization due to problems with lifetime and degradation. CO_2 contamination causes expensive additional system integration like air scrubbers or a supply of pure oxygen.

Table 1.2 Fuel Cell Types and their operational characteristics

Type	Electrical Efficiency (%)	Power Density (kW/m^2)	Operating Temperature (°C)	Start-up Time
PEMFC	40-55	3.8-6.5	50-100	seconds-minutes
PAFC	40-50	0.8-1.9	160-210	hours
AFC	45-60	0.7-8.1	60-100	minutes
MCFC	50-60	0.1-1.5	650-800	hours
SOFC	50-65	1.5-2.6	800-1000	hours

An economic simulation has illustrated typical fuel cell technology should reach to target cost of €350-625 kW^{-1} with a life time of 2.5 years to be viable (Staffell et al., 2008). When this life time period can be increased, savings will increase making costs more favorable for the market. As a result, PEMFC technology is very close to achieve this target as shown in Table 1.3 with life time up to 2.2 years and target sale price of € 220-420 kW^{-1}. Also, PEMFC has highest potential to realize required improvements due to being focus of the majority of R&D studies and commercial activity with widespread usage capability.

Table 1.3 Fuel Cell Price, Life Time and Efficiency Comparison

	Staffel et al. (2008)		Andujar et al. (2009)	
Type	Target Sale Price	Estimated Life Time	Commercial Fuel Cells	Efficiencies
PEMFC	€ 220-420 KW^{-1}	0.8-2.2 years	(BPS) € 10000 KW^{-1}	34%
PAFC	€ 660-1100 KW^{-1}	3.5-6.0 years	(ONSI) € 5000 KW^{-1}	38%
AFC	€ 120-230 KW^{-1}	0.5-1.1 years	-	-
MCFC	-	-	(MTU) € 8000 KW^{-1}	48%
SOFC	€ 510-970 KW^{-1}	1.7-5.4 years	(SWPC) € 20000 KW^{-1}	47%

BPS: Ballards Power System

ONSI: trading name of joint venture between UTC fuel cells and Toshiba

MTU: MTU onsite energy

SWPC: Siemens WestingHouse Power Cooperation

As a general definition, fuel cell is an electrochemical energy conversion device which uses hydrogen and oxygen to form direct electricity and water with supplying heat to the surrounding as shown in Figure 1.4 (Andujar et al, 2009). In a typical fuel cell system, hydrogen and oxygen fuels are fed from the anode and cathode sides of the cell respectively. The components of a typical fuel cell are bipolar plates, gas diffusion layers, electrodes and membrane. MEA (membrane electrode assembly) is the special name for the sandwiched form of anode electrode (GDL-gas diffusion layer, catalyst layer), membrane and cathode electrode (GDL, catalyst layer). Each component's operating principle and design properties are discussed in Chapter 2.

The reactions at cathode compartment and anode compartment given on Figure 1.4 are as follows;

At the anode side: $H_2 \rightarrow 2\ H^+ + 2e^-$ (1.1)

At the cathode side: $\frac{1}{2} O_2 + 2\ H^+ + 2e^- \rightarrow H_2O$ (1.2)

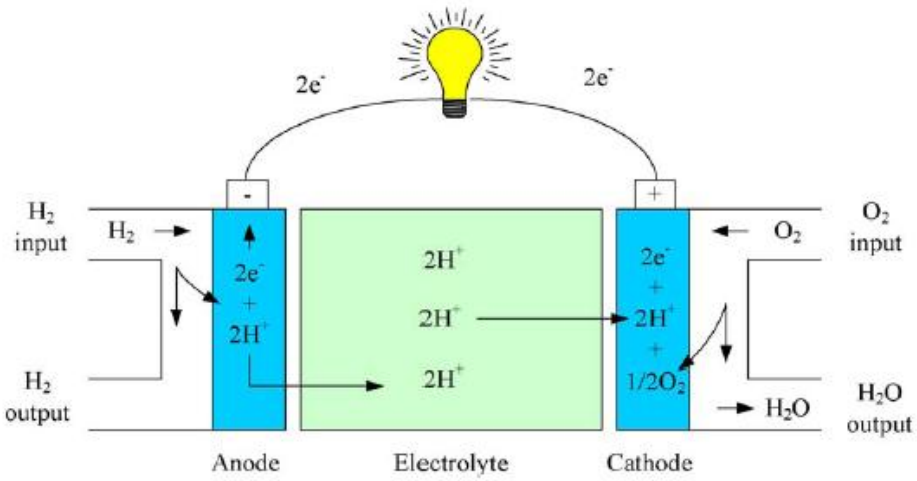

Figure 1.4 PEMFC principles of operation

PEMFC technology needs a noble-metal catalyst. The best catalyst to separate the hydrogen's electrons and protons is platinum which brings high costs to fuel cell technology. Thus, the recent studies on the PEMFC are continuing on the platinum incorporated composite catalysts. To prepare a catalyst with high efficiency, the best alternative is carbon support materials with porous structure and high surface area specialities. The porous materials are classified into three categories according to IUPAC nomenclature. If materials pore sizes is less than 2 nm, it is known as microporous material. Mesoporous material pore sizes are between 2 and 50 nm and macroporous material has the pore sizes greater than 50 nm (Yu et al, 2006). Also, the synthesized catalyst should have some fundamental physical properties to provide high efficiency. The particle size is a key point for the catalyst. It should be small enough to have uniformly distributed particles on the support's pores known as active sites where the catalysis reaction takes place. The pores should also permit the diffusion of the reactant gases and back diffusion of the product water. In fact, the best support should have a high surface area and good crystallinity morphology, provide high electrical conductivity, lower carbon corrosion and high stability in fuel cell environment for longterm operations, and synthesis method of the support material should be simple and not too expensive (Antolini, 2008).

Porous carbon support material synthesis have been developed using physical and chemical activation processes, catalytic activation of carbon precursors using metal salts or organometallic compounds, carbonization of polymer blends or polymer aerogel (Lee et al., 2006). In fact, porous carbon support synthesis has been very challenging. Then, template concept was developed by Knox and co-workers. Synthesis of porous carbon materials with uniform pore sizes is possible with various inorganic templates such as silica nanoparticles (silica sol) , zeolites, anodic alumina membranes, and mesoporous silica.

Carbon support materials having high surface area is a requirement for high loading Pt/C catalysts. When carbon material exhibits high surface area, the concentration of the solution involving the platinum dispersed per centimeter squared support surface would be low (Hou et al., 2003). Thus, the agglomeration on high surface area carbon in the course of platinum particle formation occur less than low surface area carbon. Dispersion of the catalysts is influenced by both the surface-active functional groups and the pore characteristics of the carbons. Although high surface area carbons can easily accommodate a large amount of the metal phase with a high dispersion, the significant amount of micropores on the carbon support do not allow a homogeneous distribution of the catalyst particles through the support. Therefore, micropores in the support may reduce the dispersion of the catalyst (Hou et al, 2003).

The object of this study was to synthesize the hollow core mesoporous shell (HCMS) carbon support material for the PEM fuel cells. The template used for the HCMS carbon support synthesis is a solid core mesoporous shell (SCMS) silica material. Platinum nanoparticles were penetrated to the mesopores of the carbon support via microwave irradiation method. Thermal environment required for the reduction of platinum nanoparticles on carbon support material was provided by microwave power. In microwave irradiation method, heat is generated internally within the material instead of supplying from external sources which results in

penetration through the inside of the material (Bayrakçeken, 2008). Platinum impregnated carbon support materials' voltage to current responses is first examined by cyclic voltammetry tests. Then, fuel cell performance tests are conducted for the selected electrocatalysts. Prepared electrocatalysts are sprayed on the gas diffusion layers (GDLs) and anode and cathode electrodes placed at the both sides of the Nafion membrane and these layers were hot pressed to result in 5- layer sandwiched membrane electrode assembly (MEA) components of fuel cell. MEA forms are tested at fuel cell test station.

CHAPTER 2

PROTON EXCHANGE MEMBRANE FUEL CELLS

Operating principle of the typical fuel cell was first discovered in 1839 by Sir William Grove who stated that gaseous fuels could generate electricity (Barbir, 2005). After wise, polymeric membrane technology was invented by General Electric in the early sixties (Andujar et al, 2009). A private company, Perry Energy systems, demonstrated PEMFC-powered submarine in 1989. This company demonstrated first passenger car running on PEMFCs and fuel cell powered buses in 1993 (Barbir, 2005). Today, lots of car and bus manufacturers (Daimler-Chrysler, Fiat, Ford, Honda, Hyundai, Neoplan, Nissan, Mercedes Benz, Renault, Toyota, Volkswagen and Volvo), energy companies (BP, ExxonMobill ,Shell and Texaco), fuel cell manufacturers (Ballard Power System, International Fuel cells) are working on hydrogen technologies with government and associate partners (Bernay et al, 2002, Andujar et al, 2009).

2.1. System Components of a Typical PEM Fuel Cell

The heart of a PEMFC is a polymer named as *polymer electrode membrane*. In the most of the PEMFC system, commercialized Nafion® produced by DUPONT Company is in use. At the both sides of the membrane, there are porous electrodes named as *gas diffusion layer (GDL)* one of which is belonging to anode side, and the other one is belonging to cathode side. The structure is porous, because the fed gases should diffuse through the electrode and reach to the interface between the electrode

and the membrane. The second function of the GDL is to carry product water away from the electrolyte surface to prevent sintering of pores (Zhang, 2008).

The interface between the electrode and the membrane called as *catalyst layer (or catalyst surface)* where the electrochemical reactions take place. Catalyst layer may be a part of electrode or membrane which depends on the fuel cell system design. Hydrogen fuel is fed from the anode compartment and the oxidant, typically oxygen or air, from the cathode compartment. In the catalyst surface of anode side, hydrogen splits to its protons and electrons. Protons pass through the membrane that is why proton conductivity is a very critical parameter for the membrane part. Also, electrolyte serves as a barrier to gas diffusion and half cell reactions occur at the both electrodes (Haile, 2003). The electrons travel from the outside and this direct electricity can be used for an external load as seen from the Figure 2.1. At the cathode side, ions of the oxygen react with hydrogen's protons and water is produced by exothermic reaction and heat is evolved. Figure 2.1 shows nafion, platinum and hydrogen atoms at the triple region where the good contact of them is necessary to have high performances

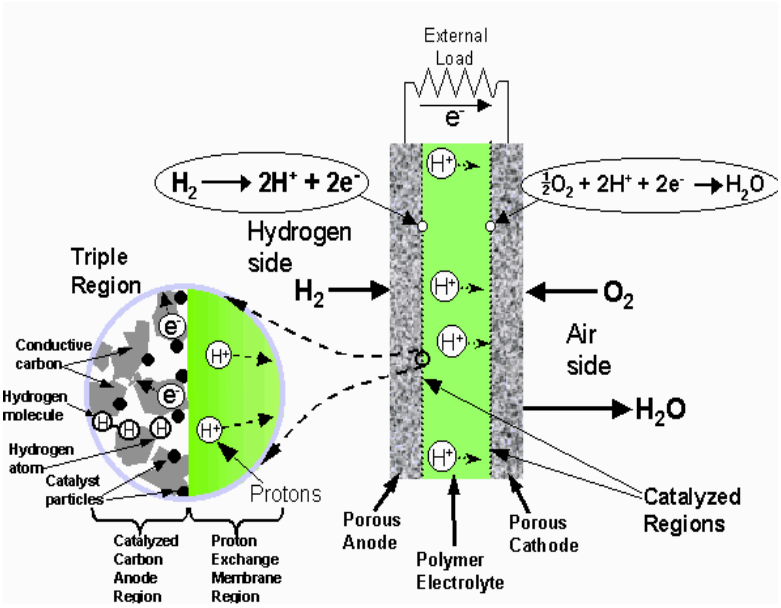

Figure 2.1 PEM Fuel Cell components and reactions

from fuel cell. As a general definition, the sandwiched structure of GDLs, catalyst layer and membrane is named as *membrane electrode assembly (MEA)*. At the both sides of the MEA, there are collector/ separator plates called as *bipolar plates* which act to collect the electrical current and separate the anode of the one cell from the cathode of the adjacent cell in the multi cell configuration (Barbir, 2005).

2.1.1. Membrane

An ideal polymer for PEMFC should exhibit excellent proton conductivity, chemical and thermal stability, mechanical strength, flexibility, low gas permeability, low water drag, low manufacturing cost and good availability. Commercially available Nafion membrane shown in Figure 2.2 is a copolymer of tetrafluoroethylene and sulfonyl fluoride vinyl ether and has a semi-crystal structure. This chemistry brings stability under oxidative/reductive conditions for long-term. Also, it acts in the reverse morphology in the dry state where ionic clusters are dispersed in a continuous tetrafluoroethylene phase. After the water absorbed by the membrane, proton-conducting channels form and conductivity increases up to a point with the water content. If the water content gets over the water tolerance of the membrane, concentration of the protons is diminished and conductivity decreases. Also, sulphonic groups of the polymers act to facilitate the transport of protons.

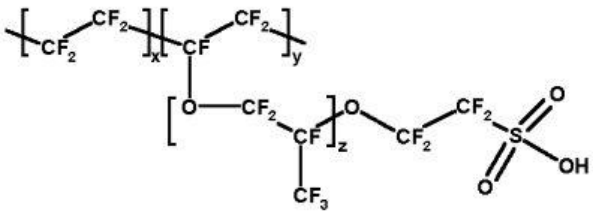

Figure 2.2 Chemical structure of Nafion

In addition, the lifetime of the membrane is very critical because it determines the life time of the cell. The thickness of the membrane should be optimized. Although the thinner layer increases proton conductivity and accordingly the

performance, mechanical strength of the membrane becomes weak and cause degradation problems (Zhang, 2008).

2.1.2. Electrodes

Platinum which is a noble metal is the best catalyst for both anode and the cathode side of the PEMFC. Due to the expensiveness of the platinum, carbon support materials were developed which provides good dispersion of platinum. High surface area property of the carbon material results in a high proportion contact between reactant gases and platinum particles. Thus, the reduction of the platinum amount is possible with achieving high loading on carbon support material. A widely used carbon- based powder is commercial Vulcan XC72® (Cobalt Company).

Catalyst layer can be a part of GDL or membrane. By the spraying method, prepared electrodes form a thin layer on the surface of GDL or Nafion. The membrane and electrodes sandwiched structure can be handled applying hot press. For that stage, Nafion helps the attachment of the catalyst layer to the membrane with applied temperature and pressure (Zhang, 2008).

2.1.3. Gas Diffusion Layer

GDLs are carbon-based porous substrates named as carbon paper or carbon cloth. The backside of the GDL which is faced with inlet gases coming from flow channels is macro-porous. The front layer of GDL which is faced with membrane is a thinner micro-porous layer composed of carbon black powder and includes hydrophobic agent to avoid flooding and to enhance intimate electronic contact with catalyst layer. An ideal GDL should exhibit effective transport of the fed gases to the catalyst surface and provide low electronic resistance and have proper hydrophobicity. Also, its surface should enhance good electronic contact with bipolar plates (Zhang, 2008).

2.1.4. Bipolar Plates

Bipolar plates have multiple functions and they are also most costly and problematic component of a fuel cell. Its primary target is to supply and distribute reactant gases to GDLs surface through flow channels. Flow channels design is state of the art issue to get well distribution of the gases on the total surface of GDLs. Bipolar plates should provide electrical connection between the individual cells. The material of the bipolar plates should be manufactured easily to prevent high costs. The stack design requires compact, stable, low weight and low corrosive materials also. Graphite is an excellent material with being light, stable and less corrosive. However, it is hard to process the flow channels and it is a very expensive solution especially for a large-scale production. Aluminum and gold coated metals are alternative solutions as a bipolar plate's raw material.

2.2. Fuel Cell Electrochemistry and Polarization Curve

Fuel cells operating principle is based on electrochemical reactions of both anode and cathode sides. Anode side of the cell is responsible from splitting hydrogen molecules into their protons and electrons according to Equation 2.1 known as hydrogen oxidation reaction (HOR). The hydrogen ions (H^+) pass through the membrane and reached to cathode side. Cathode side of the cell provides the formation of water from hydrogen's protons and the reactant gas is oxygen as stated in Equation 2.2 known as oxygen reduction reaction (ORR). Both of the reactions are taking place simultaneously on the catalyst.

At the anode side: $H_2 \rightarrow 2\,H^+ + 2e^-$ $E_a^0=0.00$ V (2.1)

At the cathode side: $\frac{1}{2}O_2 + 2\,H^+ + 2e^- \rightarrow H_2O$ $E_c^0=1.229$ V (2.2)

Overall Reaction: $H_2 + \frac{1}{2}O_2 \rightarrow H_2O$ $E_{overall}^0=1.229$ V (2.3)

ORR has a slow kinetics which dominates the entire performance of fuel cell being the one of the most limiting factors in the energy conversion efficiency. There

are many reaction mechanisms to describe ORR in aqueous electrodes. The most employed model is Damjanovic's model which describes the ORR as a multi-electron reaction where O_2 molecules in the vicinity of the electrode are irreversibly reduced directly to H_2O through 4-e^- transfer (with a constant rate, k_3) or to H_2O_2 through 2-e^- transfer (constant rate, k_1). The H_2O_2 formed can be reduced to H_2O through 2-e^- transfer (constant rate, k_2) or diffuse into the bulk solution (Vazquez-Huerta et al, 2010). These reaction mechanisms are shown in Figure 2.3, several individual reactions occur for ORR process on Pt catalysts.

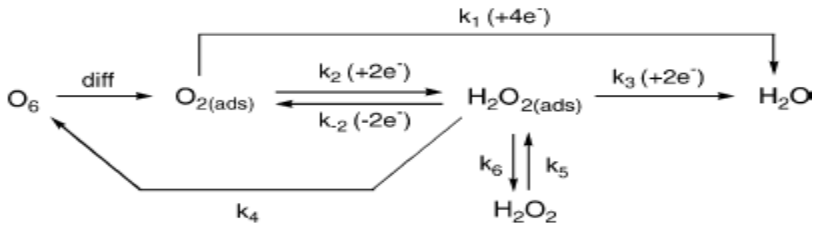

Figure 2.3 Damjanovic's oxygen reduction reaction mechanisms on noble catalyst (Wang, 2005)

The preferred route is the reduction of oxygen molecules to water by 4e^- path. However, if oxygen is reduced to hydrogen peroxide which is a harmful free radical, it causes to have lower energy conversion efficiency (Zhang, 2008).

Hydrogen oxidation reaction (HOR) has a lower oxidation overpotential and higher kinetic rate on Pt catalyst. Zhang (2008) reported exchange current density of the HOR as a $i^0_{anode} = 0.1$ Acm^{-2} and the ORR as a $i^0_{cathode} = 6$ μAcm^{-2} which proves the fast reaction kinetics of HOR. For the hydrogen-rich gas content, CO formation is inevitable, and CO tolerance of the catalysts is also an important parameter to prevent 'CO poisoning' of the adsorption sites. Platinum metal can easily adsorb CO in the anode. The best catalyst should exhibit a good CO tolerance in addition to exchange current density of the hydrogen evolution reaction. Zhang (2008) suggests that PtRu bimetallic form has excellent CO tolerance, because electronic substrate

effect and decrease the CO binding energy and activation of H_2O catalyze the oxidation of chemisorbed CO.

2.2.1. Open Circuit Voltage (OCV)

Electrical current is produced from the external movement of released electrons between anode and cathode electrodes. *Current density* is defined as direct current output of the cell over area of the electrode surface (Barbir, 2003). Measured current density of a cell is the net current value as a result of redox reactions. Barbir et al. (2003) defines *exchange current density* as a rate of redox reactions at equilibrium. Exchange current density depends critically on electrode catalyst loading, catalyst surface area and thickness of the catalyst layer (Barbir, 2003). Also, higher activity on electrode's surface results in an increase of exchange current density. It is also causes to lower the energy barrier that the charges faced with while passing from electrolyte to catalyst surface (Barbir, 2003).

At the standard conditions, theoretical hydrogen/oxygen fuel cell potential is 1.23 V as seen from Equation 2.3.When gases fed to the system and run the cell with a load but without closing the external circuit, the cell potential is expected to be at theoretical value. However, it is lower than theoretical potential due to the losses in the fuel cell, and this voltage response is known as open circuit voltage (OCV). Those losses could be originated by combined effects of fuel crossover, internal short and parasitic oxidation reactions of cathode side (Zhang, 2008). When the external circuit is closed and run the cell with a load, the potential of the cell drops even more according to net generated current. These additional losses in a typical fuel cell occur due to kinetics of the electrochemical reactions, internal electrical and ionic resistances, difficulties in transport of the reactants to reaction sites, internal currents and crossover of reactants (Barbir, 2003).

The design of the fuel cell stack includes lots of parameters and requires a detailed optimization study. In fact, the power output of a cell depends critically on materials properties and structures, configuration, and operating conditions such as

gas flow rates, pressure regulation, heat and water management. All these parameters should be optimized over a wide range of current to prevent any degradation of performance (Zhang, 2008).

2.2.2. Polarization Curve and Voltage Losses

While the fuel cell operates, the actual cell voltage is less than the OCV. *Cell voltage* defines the actual voltage of the cell. The current of the cell is equal to the current of the stack due to serial multicell configuration of the cells. Current flow causes the polarization of the anode and cathode electrodes. While the electrode potential of anode side move to a more positive value, electrode potential of cathode side move to a more negative value. This causes in a decrease of cell voltage known as voltage loss (Zhang, 2008).

Polarization curve is the plot of voltage response of the cell versus current density. In the Figure 2.4, (Bayrakceken, 2008), typical polarization curve is given. Examination of the polarization curve, performance criteria and the reason of the losses can be comment. By performing fuel cell test, many parameters effect the result of polarization curve such as gas compositions, flow rates, temperature of the cell, relative humidity (RH) and temperature of the humidifier.

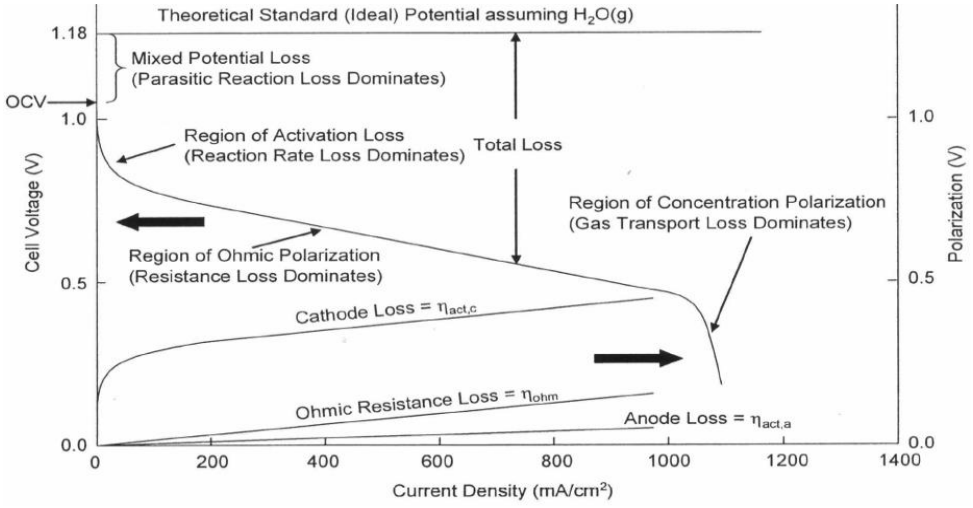

Figure 2.4 Typical fuel cell polarization curve

Voltage losses of a typical fuel cell can be classified as activation polarization, ohmic polarization and concentration polarization. Sluggish kinetics of ORR process results in a sharp drops at low current densities in the region of activation polarization. The two resistances caused to ohmic polarization comes from the flow of ions in the electrolyte and the flow of electrons through the electrode. For the higher current density, mass transfer limitations due to the transport limit of reactant gases through the pores of GDLs, electrocatalysts and accordingly, cell potential drops dramatically (Zhang, 2008).

2.3. PEM Fuel Cell Electrocatalysts and Catalyst Layers

Since platinum metal is a very expensive material as a pure electrocatalyst, synthesis of alternative support materials were examined by scientists. The best solution comes from the usage of carbon support materials. Carbon support technology provides important advantages such as determining particle size, well distribution of supported catalyst nanoparticle and has significant effects on catalytic performance and stability of the supported catalyst (Fang et al, 2008). The best support material should exhibit some characteristics such as inertness in chemical and electrochemical environment of fuel cell, large surface area for good dispersion of platinum particles, convenient porosity to allow efficient diffusion of reactant gases and products, high electrical conductivity and low cost. Carbon is the best option satisfying most of these requirements. Carbon support material has a significant effect on the cost reduction. In fact, high surface area property of the carbon support material may result in a high dispersion of platinum nanoparticles which causes high electrocatalytic activity. By this way, it is possible to increase platinum amount on carbon material while reduction of the noble metal loading for electrodes of fuel cell is also possible simultaneously. Accordingly, increase of platinum amount on carbon material may result in decrease of cost and generation of higher power density. Pt or bimetallic alloy supported on commercially available carbon black Vulcan XC-72 (VC) has a wide usage as an electrocatalysts in PEM fuel cell applications due to its relatively high catalytic activity and excellent

chemical stability in fuel cell environment. However, Fang et al. (2008) states that VC's pores are very small to be filled with electrolyte polymer and even metallic nanoparticles are trapped into micropores where triple-phase boundaries could not occur between gas, electrolyte and electrode. As an alternative to a commercial VC, there are many types of carbon support materials such as carbon nanotubes, graphitic carbon nanofibers, carbon nanocoils, macroporous carbons, mesostructured carbon materials, carbon microbeads and hollow core mesoporous shell carbon capsules.

However, it was a very restrict process to synthesis porous carbon until template synthetic procedure was discovered by Knox and his co-workers. Also, there has been lots of research on the formation of core-shell composite materials and capsules with using spherical nanoparticles as molds. Many processes were developped to synthesize uniformly distibuted and stable colloidal particles. Caruso and coworkers have introduced a method to develop many core-shell material type with layer-by-layer self assembly.

Yu et al (2002) reported that both hard core spheres and hollow shells can be produced with the removal of core templates. The main steps of porous carbon synthesis include; 1) carbon precursor and inorganic template composite preparation, 2) carbonization process, and 3) inorganic template removal. The logic behind is shown in Figure 2.5 (Lee.J. at al, 2006).

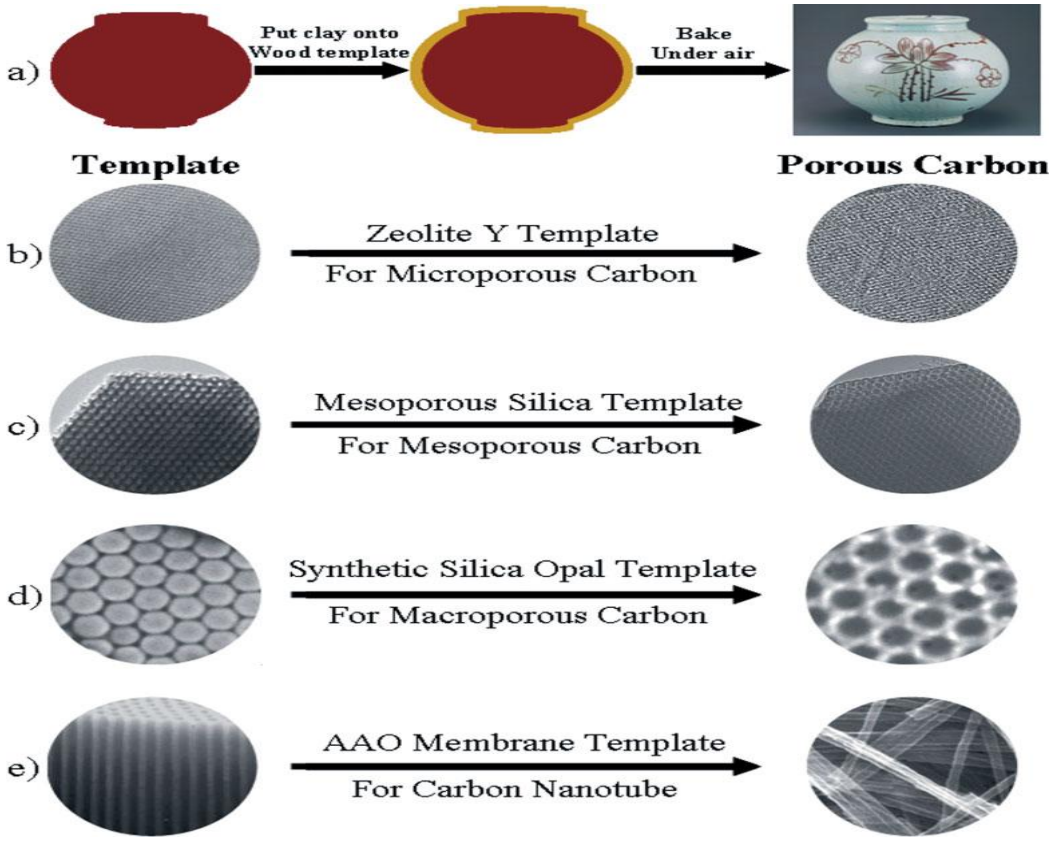

Figure 2.5 Schematic illustration of template concept for the porous carbon material synthesis (Lee et al, 2006)

In this study, to synthesize hollow core mesoporous shell carbon (HCMS) carbon capsules, mesoporous silica template named as solid core mesoporous shell (SCMS) silica spheres were used.

2.3.1. SCMS Silica Template Material

The synthesis of submicrometer-size solid core/ mesoporous shell (SCMS) silica spheres were reported by Unger et al. from the simulteneous sol-gel polymerization of tetraethoxysilane (TEOS) and octadecyltrimethoxysilane (C18TMS) (Yu et al, 2002). SCMS silica templates are forming with generating mesoporous silica layer on each silica particle by co-hydrolysis and subsequent condensation reactions of tetraethoxysilane (TEOS) and octadecyltrimetoxysilane

(C18TMS). The C18TMS acts as a porogen to generate porosity in the shell and TEOS is the silica source for the reaction medium. Equations 2.4 and 2.5 show the mechanisms of co-hydrolysis and condensation reactions (Yoon et al, 2003). The final step was the calcination under oxygen flow to remove organic groups from the structure (Yu et al, 2002).

Co-hydrolysis Reaction:

$$Si(OC_2H_5)_4 + H_2O \xrightarrow[NH_{3,alcohol}]{} Si(OH)_4 + 4\,C_2H_5OH \quad (2.4)$$

Condensation Reaction:

$$Si(OH)_4 \xrightarrow[NH_3,alcohol]{} SiO_2\downarrow + 2H_{2O} \quad (2.5)$$

It is important to control pore characteristics such as the core size and shell thickness, which affect the material storage and releasing properties. HCMS carbon support materials' core sizes and shell thicknesses should be controlled by changing the core sizes and shell thicknesses of SCMS silica templates (Fang et al, 2008). In the first step, solid core diameters of the silica spheres can be controlled by the amount of added TEOS into the aqueous ammonia solution step (Yoon et al, 2003). Fang et al. (2008) reported that shell thickness can be varying by adjusting the ratio of TEOS and C18TMS addition in the second step. Additionally, ammonia acts as a catalyst of the cohydrolysis and subsequent condensation reactions during the silica sphere formation. Also, ethanol is using as a cosolvent to form a homogenous solution (Unger et al., 1998). Temperature is another factor which affects the stability of the silica sphere formation. During the SCMS synthesis, temperature was taken under control at 30ºC. If the temperature increases more than 30ºC, the silica sphere's surface area increases accordingly. After co-hydrolysis and condensation reactions were completed, the porous shells were synthesized. To remove the organic group from structure, calcination process was performed which makes up the final SCMS structure.

2.3.2. HCMS Carbon Support Material

To synthesize carbon capsules with mesoporous shell and hollow core, it was using silica spheres composed of solid core and mesoporous shell (SCMS) structure as template. In the figure 2.6, schematic illustration of the HCMS carbon support was reported (Lee et al, 2006).

After Stöber silica spheres were prepared and formed hard core/ mesoporous shell silica structure with porogen effect, carbon precursor were incorporated to the SCMS silica templates. Fang et al (2008) reported typical carbon precursors as pitch, furfuryl alcohol, divinylebenzene and phenol.

After polymerization, resulted structures were calcined under nitrogen flow and with a ramp heating for carbonization step. Etching process of the carbon/silica composite material aims to remove silica and to have pure HCMS carbon material. Mechanism of the etching process by HF acid can be seen from Equation 2.6.

$$4\ HF + SiO_2 \rightarrow SiF_4 + 2\ H_2O \qquad (2.6)$$

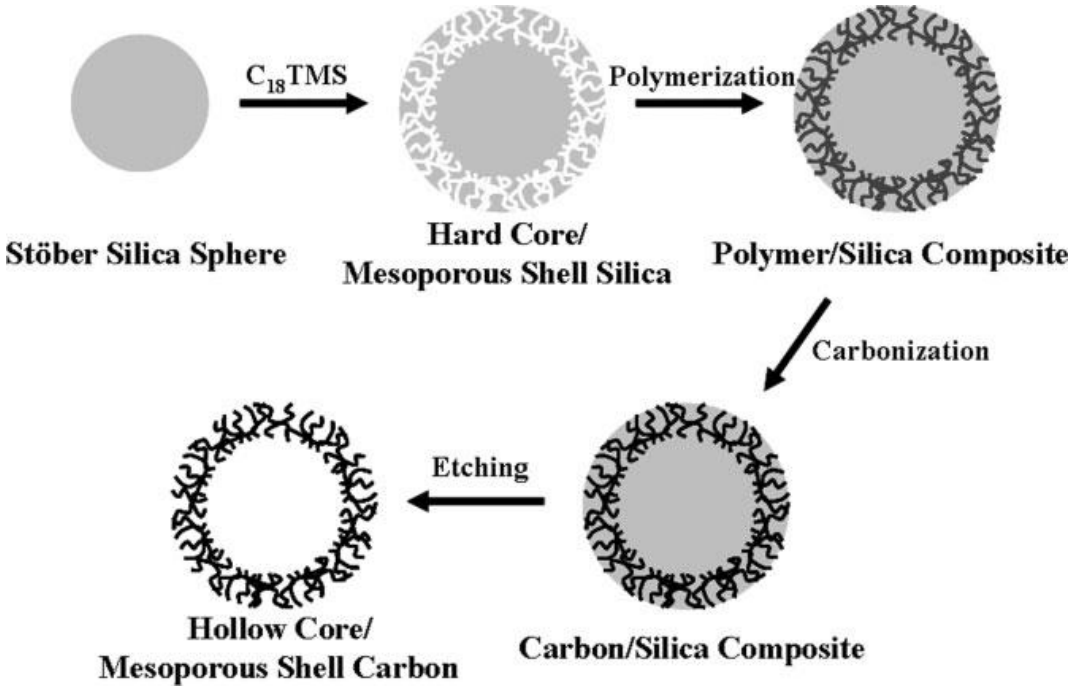

Figure 2.6 Schematic illustration for the synthesis of hollow core mesoporous shell carbon capsules

It is reported by Yu et al (2002) that the specific surface area of the HCMS carbon capsules was 1166 m^2/g for the literature BET adsorption measurement and the total pore volume was 1.47 cm^3/g. Also, elemental analysis of the HCMS carbon capsules showed that C: H molar ratio was about 23 (C98 wt % and H 0.36 wt %.). In addition, some commercial carbon support such as multi wall carbon nanotube (MWCNT) and two different carbon blacks as BP2000 and Vulcan XC72R have total surface area of 300, 1450 and 232 m^2/g, respectively (Bayrakçeken, 2008). Although, particle sizes obtained were about in the range of 1-2 nm, and the platinum utilization for the Pt incorporated BP2000 and Vulcan XC72R were 36 and 62%, respectively (Bayrakçeken, 2008). The reason for the lower platinum usage in the BP2000 carbon black can be explained by the structural difference coming from the high surface area which inhibits the accessibility of the electrolyte to the catalyst layer.

For the future research studies, it is important to increase the mesopore ordering without loss of the particles' uniformity and monodispersity, and how to control the thickness of the outer shell as well as the particle size. The impregnation of metallic nanoparticles onto carbon support pores, enlarging the pore size of the mesoporous shell without distorting the particle morphology is another important aspect.

2.3.3. Platinum Impregnation Methods

To impregnate platinum onto carbon support material, there are different methods such as impregnation, micro emulsion, sequential and co-precipitation, supercritical carbon dioxide deposition, microwave irradiation, ion exchange, sol gel, ultrasonication (Bayrakçeken, 2008).

In microwave irradiation method, the internal energy is supplied by microwave power which provides heating the material's inside and outside simultaneously. Reducing agents such as ethylene glycol, hydrazine, sodium borohydrate and urea are using which absorb microwave energy. The advantages of microwave heating method are the opportunity to supply high energies in shorter duration and satisfying inside heating of material in molecular scale.

In the Table 2.1, the literature studies to achieve high Platinum loading were summarized. Fıçıcılar et al (2009) achieved 20 wt % platinum loading on HCMS carbon support material by using ethylene glycol as a reducing agent via microwave irradiation method. Kim et al (2006) reached 40 wt % platinum impregnation on commercial carbon support; Vulcan XC, by using an additional reducing agent $NaBH_4$ with a combination of ethylene glycol.

Fang et al (2009) studied ethylene glycol, $NaBH_4$ and urea as a reducing agent and achieved 60 wt % platinum impregnation on commercial carbon support; Vulcan XC. In the case of ethylene glycol, Fang et al (2009) used microwave irradiation method where reducing agent amount and supplied microwave inlet power was higher than Bayrakçeken et al (2009)'s study.

Table 2.1 Platinum Impregnation Methods on Carbon Support Materials

Author	Method	Experimental	Result
Fang et al (2009)	HD-EG Method /urea assisted EG process	-300 mg of urea (i.e., molar ratio of urea/Pt) 20) -200 mL of EG was added -the solution was heated to 120 °C, kept for 1 h, and stirred overnight.	Pt (60 wt %)/VC catalyst was prepared.
Fang et al (2009)	$NaBH_4$ reduction	-The $NaBH_4$ aqueous solution was added (the molar ratio of $NaBH_4$ to Pt was set at 10). -stirring overnight	Pt (60 wt %)/VC catalyst was prepared.
Fang et al (2009)	EG-MW synthesis	-200 mL of EG was added, and the mixture was adjusted to pH 7-8 by dropwise addition of 0.4 M KOH. -the solution was heated in a household microwave oven (700 W) for 5 min.	Pt (60 wt %)/VC catalyst was prepared.
Kim et al (2006)	$NaBH_4$ -assisted ethylene glycol reduction	-(molar ratio of ethylene glycol:NaBH4 = 10:1) was slowly added with vigorous stirring. -After stirring for 4 h at room temperature, an aqueous solution of HCl was added.	Pt (40 wt %)/VC catalyst was prepared.
Fıçıcılar et al (2009)	EG-MW synthesis	-50 mL EG was added and the mixture was mixed ultrasonicly for 30 min. -the solution was heated in a household microwave oven (800 W) for 120 sec.	Pt (20 wt %) HCMS catalyst was prepared.

HD: Homogeneous deposition

EG: Ethylene Glycol

Ethylene glycol exhibits high permanent dipole with high dielectric constant (41.4 at 25 °C) and dielectric loss which makes it an excellent susceptor for microwave irradiation method (Kerner et al. 2000 and Komarneni et al., 2002). In addition, ethylene glycol acts as a solvent in microwave-assisted reactions with preventing arching. If arching is occured, it leads to the decomposition of solvents which results in high level of impurities due to the yield of carbon and carbonaceous residues (Kerner et al, 2000).

Reaction mechanisms of platinum impregnation include reduction of the precursor in conjuction with the oxidation of ethylene glycol. Due to being very weak acid (p*K*a ≈ 15[13]), ethylene glycol can be easily oxidized to aldehydes, carboxylic acids, and CO_2 according to below mechanisms:

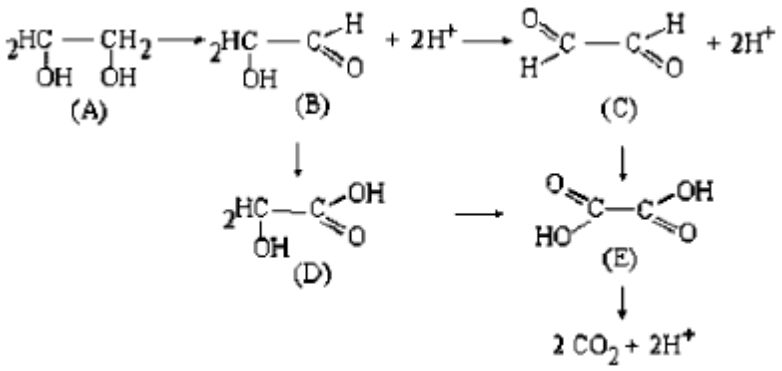

(2.7)

For stage A, -OH groups of ethylene glycol interact with Pt- ion sites which results in the oxidation of alcohol groups to aldehydes as shown in stages B and C. These aldehydes can be easily oxidized due to low stability of the structure and forms glycolic acid (stage D) and oxalic acid (stage E). These two carboxylic acid groups in stage E may be further oxidized to CO_2 or carbonate in alkaline media. Accordingly, electrons donated from these oxidation reactions result in the reduction of the Pt metal ions (Bock et al., 2004). As a parallel or alternative reaction pathway, the oxidation of ethylene glycol could take place due to the platinum well known

ability of abstracting hydrogen from carbon atoms as shown in below reaction mechanism (Bock et al, 2004).

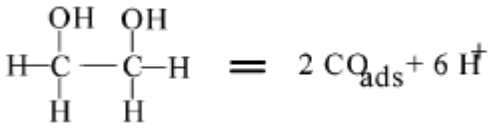

(2.8)

2.4 PEMFC Electrocatalyst Degradation

PEMFCs are believed to be the most convenient fuel cells for the portable and mobile applications. It is essential to construct the PEMFCs with suitable components that they can operate for long time periods which can compete with the conventional systems. There are still some drawbacks related with the durability of fuel cell components under operating conditions. It is known that the PEMFC components are getting degraded during the fuel cell operation which causes performance losses.

The heart of a PEM fuel cell is MEA so the degradation occur in the MEA may cause drastic performance losses. The proposed degradation reasons in MEA are: (i) activity loss of the electrocatalyst; (ii) carbon corrosion; or (iii) degradation of the polymer electrolyte membrane and ionomer in the catalyst layer by the formation of hydrogen peroxide and the generation of heat. It is believed that the most significant ones among these is the activity loss of the electrocatalyst (Kim et al., 2008). The factors which cause electrocatalyst degradation may be Pt agglomeration/sintering, Pt dissolution (Chung et al., 2009) and carbon corrosion which can occur during the operation of the fuel cells (Seo et al., 2010, Chen et al. 2009).

Pt nanoparticles impregnated over high surface area carbon supports are used as the electrocatalysts in PEMFCs. Due to their high specific surface energy, nanoparticles tend to agglomerate into bigger particles which will minimize their surface energy and the electrochemical activity simultaneously slows down. Pt can also dissolve from the carbon support. These agglomeration/dissolution processes are

accelerated under harsh operating conditions, which may result in a decrease in the number of active sites and hence a decreased electrochemical active surface area of the electrocatalyst, which will directly lead to performance loss in PEM fuel cells (Zhang et al., 2009). PEMFC has harsh operating conditions for both anode and cathode parts of fuel cell. While anode catalysts are exposed to a strong reducing hydrogen atmosphere, cathode catalysts are under strongly oxidizing conditions due to high oxygen concentration, high potential (>0.6V versus the standard hydrogen electrode (SHE), and sometimes to see too high potentials (e.g., >1.2 V) for short periods of time), which may accelerate the degradation of the electrocatalysts (Shao et al., 2007). The schematic representation of Pt agglomeration/dissolution is given in Figure 2.7.

The corrosion resistance of the support material is also very important in the durability of the PEM fuel cells. In an electrochemical system, carbon oxidation is often observed according to the following reaction:

$$C+H_2O \rightarrow CO_2 + 4H^+ + 4e^- \quad (2.7)$$

The thermodynamic potential of this carbon oxidation reaction is 0.207 V. Accordingly, the electrochemical oxidation of the carbon is thermodynamically possible for fuel cell operations above 0.2 V (Shao et al., 2007). The surface chemistry of the carbon changes via electrochemical corrosion of the carbon surface. Carbon oxidation may lead to detach some Pt particles from the carbon support resulting in a decrease of catalytic activity and the interaction between carbon support-Pt may be weakened (Wang et al., 2007). Wang et al. (2007) investigated the corrosion of BP2000 and Vulcan XC72 by applying a fixed potential of 1.2 V and they observed surface oxide formation which was attributed to the hydroquinone-quinone (HQ-Q) redox couple on the carbon black surface given by:

$$C{=}O + e^- + H^+ \leftrightarrow C{-}OH \quad (2.8)$$

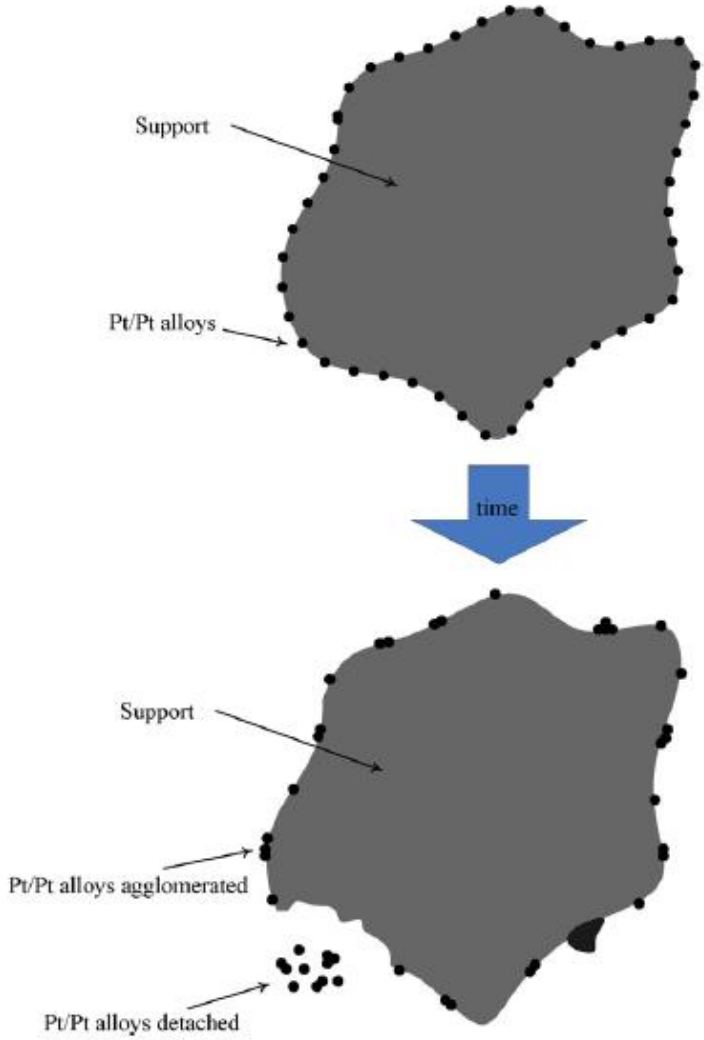

Figure 2.7 Schematic representation for Pt agglomeration on and Pt dissolution from support material surface (Shao et al., 2007)

They found that the amount of HQ-Q redox couple (the current peak resulting from the surface oxide formation due to this redox reaction) on BP2000 was about 1.5 times that on Vulcan when normalized by the electrochemically active area. The cyclic voltammograms for two different carbon supports, Vulcan XC 72 and BP2000, after potential holding @1.2 V is given in Figure 2.8 (Wang et al., 2007). As the potential holding time increases HQ-Q redox couple increases which means that carbon corrosion increases.

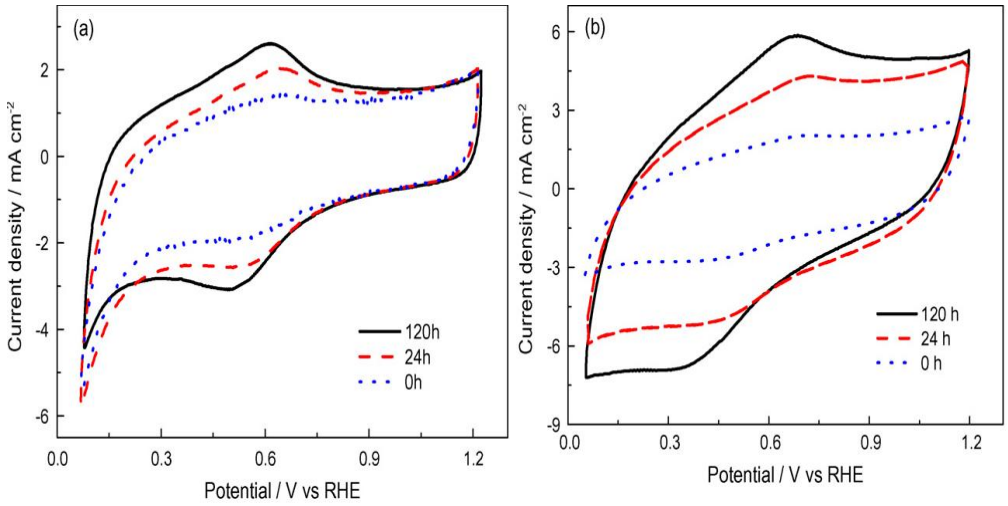

Figure 2.8 Cyclic voltammograms recorded after a) Vulcan b) BP2000 electrodes hold @ 1.2 V for 0, 24 and 120 h in 0.1 M H_2SO_4

CHAPTER 3

EXPERIMENTAL

As a major target, hollow core mesoporous carbon materials were synthesized with two stage procedure. In the first stage, solid core mesoporous shell (SCMS) silica templates were synthesized. In the second stage, these synthesized SCMS silica samples were used to synthesize HCMS carbon. HCMS carbon synthesis was followed by two separate routes named as 'phenol/paraformaldehyde route' and 'Divinylbenzene/AIBN route'. After having high surface area and mesoporous textured carbon samples, Platinum (Pt) was impregnated by the microwave irradiation method. Prepared catalysts were then physicochemically and electrochemically characterized. The stability of the prepared catalysts were also investigated by using cyclic voltammetry. The process stages are explained in details at the experimental subsections.

3.1. Synthesis Materials

Tetraethoxysilane; TEOS (98%, ACROS) was used as a silica source for the SCMS silica template synthesis. Ammonium hydroxide, NH_4OH (~28-30%, ACROS) was used as the catalyst for hydrolysis and condensation reactions of colloidal silica spheres. Deionized water and ethanol (99.8%, Riedel-de Haen) were acting as co-solvents. Octadecyltrimethoxysilane, C18TMS (90% tech., Aldrich) was used as the porogen for the sol-gel polymerization reactions. Oxygen gas was used to remove organic groups of octadecyltrimethoxy-incorporated silica material by calcination process.

In the HCMS synthesis followed by the first route, Phenol (99.5%,Merck) and Paraformaldehyde (95%, Merck) were used as the carbon source. Aluminum Chloride Hexahydrate (99%, Fluka) was used to form acidic catalytic sides before attaching phenolic resins. In the second route, Divinylbenzene (80%, Aldrich) was used as the carbon source and Azoisobutyronitrile (98%, Acros) was the initiator for DVB. Carbonization of polymerized carbon structure was achieved under nitrogen gas flow by calcination. Hydrofluoric acid (48%, Merck) solution was used for the etching of the carbonized samples.

3.2 Solid Core Mesoporous Shell (SCMS) Silica Templates Synthesis

The experimental setup for SCMS synthesis is given in Figure 3.1. The setup consisted of a 250 ml balloon flask with two necks which was immersed in a water bath, a Pt type thermocouple equipped GEMO DT-742 temperature controller, a magnetic stirrer (Heidolph MR 3001) to apply vigorous stirring and heating during the course of hydrolysis and condensation reactions. The synthesis of SCMS silica template starts with the formation of colloidal silica spheres. 3.14 ml of aqueous ammonia (32 wt %) was added into a solution which contains 74 ml of ethanol and 10 ml of deionized water. When the mixture reached to 30 °C, 6 ml of TEOS was added under vigorous stirring and the reaction mixture is kept stirring for 1 h to yield uniform silica spheres (Stöber silica sol). A mixture consisting of 5 ml of TEOS and 2 ml C18TMS was added into the colloidal solution containing silica spheres and further reacted for 1 h. To precipitate the solution, centrifugation technique was used. The centrifugation was applied three times with the addition of deionized water to reduce the pH (6000 rpm, 15 min for each turn). Then, the precipitate is dried in the vacuum oven for 12 h at 353 K. The resulting octadecyltrimethoxy-incorporated silica-shell /solid core nanocomposite is further calcined at 823 K for 6 h under oxygen atmosphere to produce SCMS silica material finally.

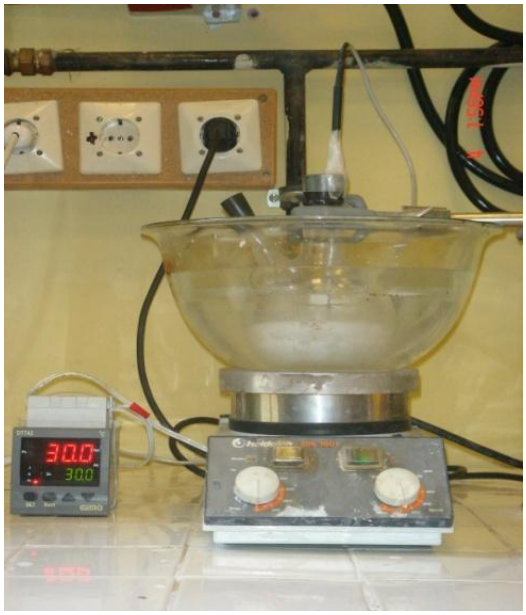

Figure 3.1 Experimental setup for SCMS silica synthesis

3.3 Hollow Core Mesoporous Shell (HCMS) Carbon Support Synthesis

Two different routes were followed in order to synthesize HCMS carbon support. The former one is based on the utilization of phenol/paraformaldehyde precursor and the latter one is on divinylbenzene precursor as the carbon source.

3.3.a Phenol/Paraformaldehyde Route

Aluminum is incorporated into the silica template via an impregnation method to form acidic sides for phenolic resin attachment. 1 g of SCMS silica is added to an aqueous solution containing 0.27 g of $AlCl_3.6H_2O$ in 0.3 ml water. The resulting slurry is stirred for 30 min and then the powder is dried in air at 353 K. The Al-impregnated SCMS silica is calcinated at 823 K for 5 h in air to yield the SCMS aluminosilicate. 0.374 g of phenol per gram of the SCMS aluminosilicate template is incorporated into the mesopores by heating at 373 K for 12 h under static vacuum. The resulting phenol-incorporated HCMS aluminosilicate is reacted with paraformaldehyde (0.238 g) at 403 K for 24 h inside the mesopores to yield phenol-

resin/HCMS aluminosilicate nanocomposite. The resulting nanocomposite material is heated at 1 K min^{-1} to 433 K and held at that temperature for 5 h under nitrogen flow. The schematic representation for HCMS carbon support synthesis by Phenol/Paraformaldehyde route is given in Figure 3.2.

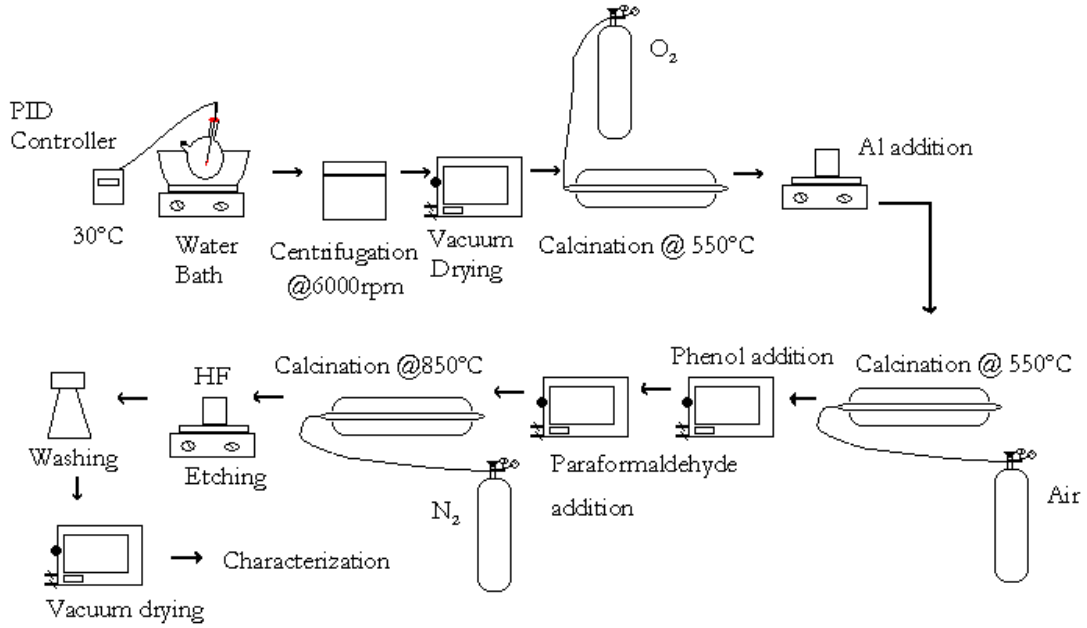

Figure 3.2 Schematic illustration of the overall process for HCMS carbon support synthesis by Phenol/Paraformaldehyde route

3.3.b Divinylbenzene/AIBN Route

Divinylbenzene which was a carbon source was used with a free radical initiator named as Azoisobutyronitrile (AIBN). The powder SCMS silica templates were dehydrated in a vacuum oven at 200 °C overnight. For 1 g of SCMS silica templates, DVB and AIBN were incorporated at molar ratios of 22, 24 and 26. Different molar ratios were tried to examine the effect of this parameter on the physical properties of the synthesized HCMS carbon support such as its surface area, pore size distribution, and pore volume. Freeze-pump-thaw cycles were performed several times to remove the dissolved oxygen from the resulting DVB-incorporated SCMS silicate containing AIBN. Three freeze pump setup, as given in Figure 3.3,

was constructed with a schlenk glass tube with a valve and thermos bottle including liquid nitrogen. Glass tube connected to a vacuum pump to remove the oxygen gas formed during the reaction. The system was run more than three cycles for each sample. For each cycle, glass tube was dipped into liquid nitrogen for 5 minutes and then removed to atmosphere and waited at least 15 minutes until the dissolution of frozen sample.

Figure 3.3 Three-freeze-pump setup

The samples were then polymerized overnight in the oven at 70°C under nitrogen atmosphere. The resulting cross-linked structure was calcined under nitrogen flow at 1103 K for 8 h with a ramp of 1 K min^{-1} for further carbonization. Silica frameworks from the calcined nanocomposite material were removed by etching with 48 % HF and after washing under vacuum the resulting material is dried.

3.4 Catalyst Preparation

The synthesized HCMS carbon was used as the carbon support for the PEM fuel cell electrocatalyst. Microwave irradiation method was used to prepare the catalysts.

3.4.1 Materials

Hydrogen hexachloroplatinate (IV) hydrate (H_2PtCl_6 x H_2O, 99.9 %, Sigma-Aldrich) was used as the Pt precursor for the catalyst preparation. Ethylene glycol (≥ 99 %, Merck) was used as the solvent and reducing agent. $NaBH_4$ (fine granular for synthesis, Fluka) and hydrazine (25 % in water, Merck) were also used as the reducing agents. Acetone (hydrate solution, Sigma-Aldrich) and deionized water was used to remove the solvent from the catalyst. A commonly used commercial carbon support, Vulcan XC 72 (Cabot), was also used for comparison.

3.4.2 Experimental Procedure

Platinum impregnation was achieved by microwave irradiation method by using a domestic microwave oven (Akai, 2450 MHz, 800 W). Microwave oven was used to supply the required heat to reduce the Pt ion coming from the precursor into its metallic form. Before the experiment, the HCMS carbon support samples were dehydrated in vacuum oven overnight. Firstly, 0.05 M aqueous solution of platinum precursor was prepared where hydrogen hexachloroplatinate (IV) hydrate was Pt complex. To achieve 40 % platinum loading on the carbon support material, required volume of 0.05 M platinum solution was taken. As a reducing agent, $NaBH_4$ and hydrazine solutions were also added to ethylene glycol. Reducing agent volumes were changed between 50-200 ml, and then 0.1 g of HCMS carbon support and platinum solution were added into reducing agent. This solution was mixed by homogenizer (IKA Ultra Turrax T 25) for 30 min. Homogenized solution was placed to microwave oven. After 2 minutes microwave duration, the sample was cooled immediately, filtered and then washed with acetone. The residue was then dried in vacuum oven overnight at 70°C. Same catalyst preparation procedure was used to prepare Vulcan XC supported Pt catalysts.

3.5 Physical Characterization

Physical characterizations of the prepared carbon supports and electrocatalysts is very important to 1) synthesize proper structure with high activity

and high selectivity, 2) recognize prepared structures, 3) investigate the mechanisms of catalysts and certain additives (Zhang, 2008). Zhang (2008) stated that electrocalatalysts have special property of good conductivity when compared with other heterogeneous catalysts which are acting as insulator. Thus, characterizations of electrocatalysts require some special techniques because of their conductivity property.

The main characterizations for carbon supports and electrocatalysts include the measurement of the surface area and pore size distribution of materials, the electrochemical active surface area, the phase and composition of active components, the particle size of active components, the morphology and crystal planes and other features (Zhang, 2008). Following methods were used to characterize the prepared electrocatalysts.

3.5.1 Brunauer-Emmett-Teller (BET) Method and Physical Surface Area

BET surface area is an important characterization technique for many types of advanced materials such as additives, battery active materials, fibers, nanomaterials, minerals, pharmaceutical materials, pigments, powder metallurgy materials and thermal spray powders. Three scientists named as Brunauer, Emmett, and Teller developed BET method optimizing the theory for measuring surface area of materials. The theoretical approach of the BET method is based on the surface of adsorbed gas molecules. Especially, nitrogen adsorption technique is applied to cover the surface of the material. In the literature, it is given that the area covered by a nitrogen molecule at liquid nitrogen temperature is 16.2 $Å^2$ (Zhang, 2008). BET analysis experiment is performing in the vacuum chamber and the amount of nitrogen molecules that covers the surface of the sample in that vacuum chamber gives the adsorption and desorption isotherms. It is assumed that only one nitrogen atom can occupy to each site of the sample and the atoms do not interact with each other. While the molecules adsorb on the surface, pressure of the vacuum chamber

will decrease. From the experiment, a series of *P* and *V* data can be obtained. According to BET equation (Zhang, 2008).;

$$\frac{\mathcal{P}}{\mathcal{V}(\mathcal{P}_0-\mathcal{P})} = \frac{1}{\mathcal{V}_m\mathcal{C}} + \frac{(\mathcal{C}-1)}{\mathcal{V}_m\mathcal{C}}\frac{\mathcal{P}}{\mathcal{P}_0} \tag{3.1}$$

where $\mathcal{P}$; equilibrium pressure

$\mathcal{P}_0$; saturated vapor pressure

$\mathcal{V}$; total volume

$\mathcal{V}_m$; volume of gas molecules corresponding to the monolayer

Plotting '$\frac{\mathcal{P}}{\mathcal{V}(\mathcal{P}_0-\mathcal{P})}$' vs '$\frac{\mathcal{P}}{\mathcal{P}_0}$' , a straight line can be obtained where the slope and intercept of this line gives '$\frac{(\mathcal{C}-1)}{\mathcal{V}_m\mathcal{C}}$' and '$\frac{1}{\mathcal{V}_m\mathcal{C}}$', respectively. Then, $\mathcal{V}_m$can be found easily.

Nitrogen adsorption and desorption isotherms which are drawn volume absorbed per gram of sample vs relative pressure, can be classified in six different type according to IUPAC classification of adsorption isotherms as shown in Figure 3.4 (Donohue et al, 1998).

Donohue et al (1998) states "Type I isotherm approaches a limiting value and usually is used to describe adsorption on microporous adsorbents. Types II and III describe adsorption on macroporous adsorbents with strong and weak adsorbate-adsorbent interactions respectively. Types IV and V represent mono and multilayer adsorption plus capillary condensation. Type VI illustrates that the adsorption isotherms can have one or more steps."

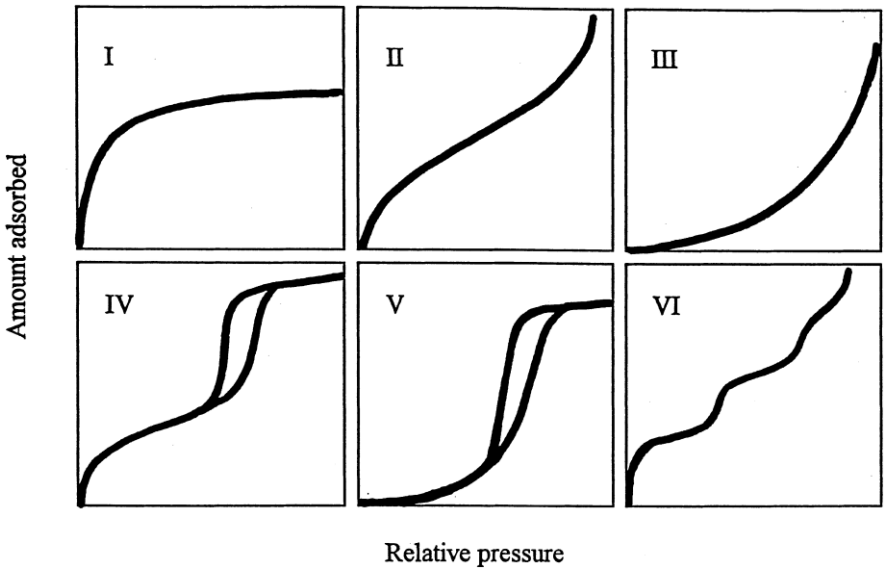

Figure 3.4 IUPAC Classifications of Adsorption Isotherms for Gas-Solid Equilibria

The specific surface area, $a(BET)$ can be obtained using BET monolayer capacity, n_m, and average area occupied by each molecule in the completed monolayer, σ, as (Rouquerol,1999);

$$a(BET) = n_m \mathcal{L} \sigma \qquad (3.2)$$

where $\mathcal{L}$; Avogadro constant

Surface areas of SCMS silica template and HCMS carbon support structures were measured by the BET method and the Langmuir surface area method. In addition, pore size distribution via adsorption and desorption isotherms, micropore volume by DA, DR, DFT, t-plot methods and gas uptake properties of materials can also be analyzed by the BET surface area instrument. Quantachrome Autosorb 6B device was used for BET surface area analysis and the samples were preheated at 350 °C for 3 hours.

3.5.2 Thermal Gravimetric Analysis (TGA)

Thermogravimetric analysis (TGA) is an analytical technique in which thermal stability and fraction of volatile components of the materials are determined by monitoring the weight change of a specimen as a function of temperature. Derivative thermal gravimetry (DTG) is a method of expressing the first derivative of TG results with respect to temperature. Thus, DTG records the rate of weight loss versus temperature ($\frac{dw}{dT}$).

TGA and DTG analysis were used to determine the percentage of Pt over the carbon supports in dried-air atmosphere. Burning the carbon support material results in the determination of the percentage of Pt impregnated onto the carbon support. The weight loss of the samples were analyzed by Perkin Elmer Pyris 1 thermal gravimetric analysis device under air atmosphere and between 25°C-980°C temperature range with a linear heating ramp as 10°C/minutes.

3.5.3 X-ray Diffraction (XRD) Analysis

X-ray diffraction is a commonly used technique to analyze the materials' crystallographic structure and chemical composition. Wilhelm Conrad Röntgen discovered X-rays in 1895. If X-rays interact with a crystalline substance, one gets a diffraction pattern without destructing the crystals. When X-ray beam is sending to a sample structure, electrons of the atomic structure start to oscillate in a same frequency with the incoming beam. If the atoms are in crystalline structure which is in a regular pattern, there will be a constructive interference and X-ray beams will leave the sample at various directions. Also, each crystalline substance has different atomic arrangements which result in diffraction of X-rays in a unique pattern. Theoretical calculation of X-ray reflections are given according to Bragg's Law as (Zhang, 2008);

$$n\lambda = 2d\sin\alpha \quad (n = 1,2,3 \ldots) \tag{3.3}$$

where λ; wavelenght of the X-rays

d; lattice spacing

α; half-value of the diffraction angle

n; order of the reflection

Crystalline phases were identified by using XRD. The XRD patterns show three main characteristic peaks of face-centered cubic (fcc) structure of crystalline Pt, which are {1 1 1}, {2 0 0}, and {2 2 0} planes (Bayrakceken, 2008). {1 1 1} and {2 0 0} peaks were overlapping and sizes of the platinum particles were calculated from the Scherrer equation using the half-full-width at half maximum of the {220} reflection. The Scherrer equation is given in equation 3.4.

$$t = \frac{K\lambda}{B\cos\theta_B} \qquad (3.4)$$

where, K is the Scherrer constant, λ is the wavelength of radiation ($\lambda_{Cu,K\alpha} = 0.154\,nm$. B is the integral breadth of peak (in radians 2θ) located at angle θ_B as shown in Figure 3.15. Accordingly, parameter B was calculated as;

$$B \approx \frac{1}{2}(2\theta_1 - \theta_2) = \theta_1 - \theta_2 \qquad (3.5)$$

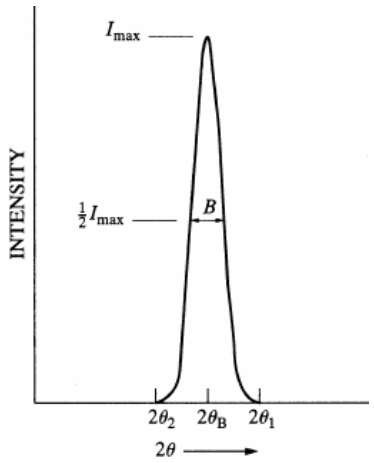

Figure 3.5 XRD pattern (Bayrakçeken, 2008)

The particle size of the Pt/HCMS catalyst was calculated from the {220} plane.

3.5.4 Scanning Electron Microscopy (SEM)

The Scanning Electron Microscope creates the magnified images in superb resolution by using beam of electrons instead of light waves. Before the analysis, samples are coated by sputter coater machine with a very thin layer of gold to make them conductive. SEM system scans the surface of the materials line by line by electron beams and electron detectors one of which measures low-energy electrons (secondary electron detector), and the other one measures high-energy electrons (back-scattered detector), provide topographic image and information about the differences in atomic number within a sample (Zhang, 2008).

The Scanning Electron Microscope (SEM) analyses were done for different SCMS silica template and HCMS carbon support samples. Quanta FEG scanning electron microscope was used with a magnification range from 15x to 200,000x (reached in 25 steps) and a resolution of 5 nanometers.

3.5.5 Transmission Electron Microscopy (TEM)

The Transmission Electron Microscope allows the user to determine the internal structure of materials rather than surface image, either of biological or non-biological origin. Although electrons that pass through the sample creates the image, those were stopped or deflected by dense atoms are subtracted from it, thus black and white image is obtained (Zhang, 2008). TEM method differs from SEM analysis in that respect. By the TEM analysis, it can be determined the size, structure, composition and arrangement of the particles which constitute the specimen as well as their relationship to each other in submicroscopic detail. Jeol 2100 F transmission electron microscope was used for TEM analysis.

3.6 Electrochemical Characterization

3.6.1 Cyclic Voltammetry (CV)

Cyclic voltammetry is a kind of potentiodynamic electrochemical measurement. CV is a commonly used diagnostic tool for the electrocatalyst characterization. This method provides a fast and convenient way to characterize the half cell reactions and get some useful data about the electrochemical activity of the electrocatalysts. The system consists of three main electrodes named as working electrode, reference ele**c**trode and counter electrode, an electrolyte and a built-in analog voltage sweep generator.

Working Electrode (WE): Working electrode used in the experiments has a surface included glassy carbon (GC) material where the prepared samples are injected on and dried there. The potential of the working electrode is being controlled by potentiostat during the experiment and also the current passing through that electrode is being measured. The system response provides current vs voltage data which reflects characteristics of the samples.

Reference Electrode: Reference electrode used in the experiments is silver-silver chloride (Ag/AgCI, CI^-) reference electrode. Reference electrode has a function of measuring the potential difference at the interface of the WE and the injected sample as accurately as possible (Bayrakçeken, 2008). In an ideal situation, no current passes through the RE, it should be stable and consist of well-known electrode potential. Due to that reason, 0.1 M potassium chloride solution is injected to the reference electrode reservoir.

Counter Electrode: Counter electrode, also called an auxiliary electrode, used in the experiments is a typical platinum wire. Counter electrode acts to create correct potential difference between the reference electrode and working electrode according to the applied linear voltage ramp.

The working principle of cyclic voltammetry is to measure the response of potential difference between reference electrode and working electrode when a linear electrode potential ramp vs. time is applied. This applied ramping is known as scan rate of the experiment which can be seen from Figure 3.6. While the potential responses are taken, the current data between the working electrode and counter electrode are measuring simultaneously by the system. If the potential and current responses of the system plotted as Figure 3.7, the information about the samples' redox potential and electrochemical reaction rates can be interpreted.

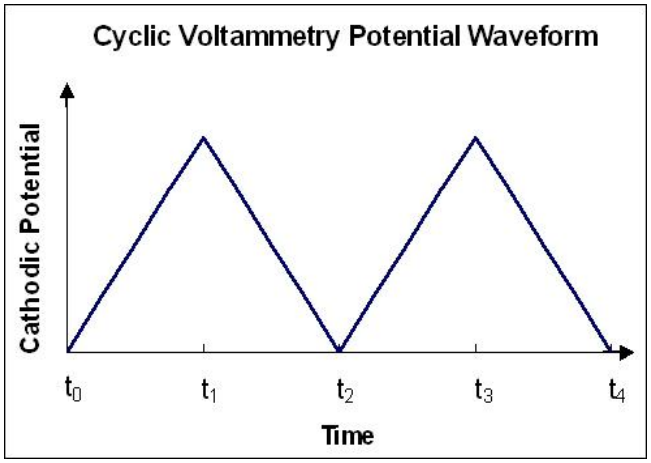

Figure 3.6 Scan rate of one cycle experiment

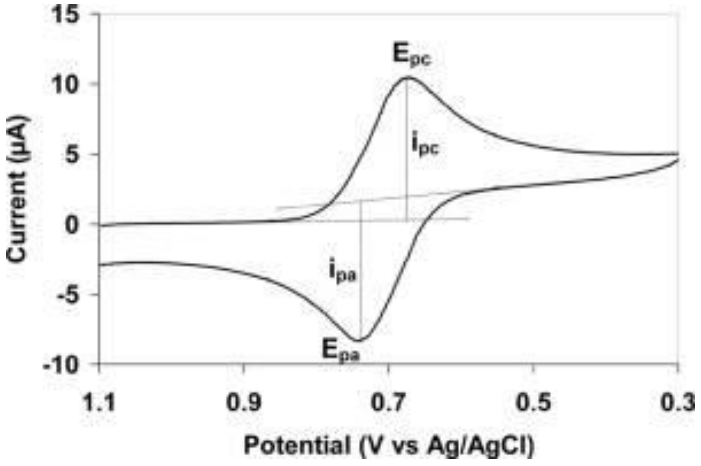

Figure 3.7 Typical cyclic voltammetry result

Prepared HCMS carbon supports, Pt impregnated carbon supports (HCMS or Vulcan XC) were characterized by cyclic voltammetry experiments. Hydrogen oxidation reaction (HOR), oxygen reduction reaction (ORR) and the stability of the electrocatalysts were investigated. A standard three electrochemical cell configuration was used during the experiments. A PEM fuel cell electrocatalyst rotating ring disk electrode (RRDE) bundle (Pine Instrument) was used. This bundle includes computer controlled bipotentiostat, GC electrode (5 mm in diameter), Pt wire, Ag/AgCl electrode, rotator, glass RDE cell and all the connections. Experimental setup is given in Figure 3.8.

Figure 3.8 Experimental Setup for Cyclic Voltammetry

The electrocatalysts in interest were covered over the GC electrode in order to determine their activity. The corresponding catalyst ink was prepared as follows: measured amounts of the prepared catalysts was mixed with deionized water, 1,2-propandiol, and 15% Nafion solution (Ion Solutions Inc.). The suspension was then homogenized for 15 minutes with a homogenizer. Then required amount from this

solution is taken and pipetted over the GC electrode and left for drying. The amount of the prepared catalysts placed in the solution was adjusted so that the metal loading per unit area on the 5 mm diameter GC electrode was 28 μg Pt cm^{-2}. 0.1 M perchloric acid (70-72 %, Merck) was used as the electrolyte during the experiments. 0.1 M potassium chloride (Merck) solution was used in the reference reservoir in order to provide the connection between the reference electrode and the electrolyte. Glass cell was filled with prepared 0.1 M perchloric acid solution. Prepared 0.1 M potassium chloride was injected by a syringe to reference electrode's reservoir and then all the connections were made before passing through the experiments.

3.6.1.a Experimental Procedure

Hydrogen oxidation reaction (HOR) and oxygen reduction reaction (ORR) were investigated by using a standard three electrode cell configuration. Cyclic voltammograms for the HOR were recorded in a 0.1 M $HClO_4$ electrolyte solution that was saturated with nitrogen for 30 min to remove the oxygen. All the cyclic voltammetry tests were performed at room temperature. CV data were reported with respect to a normal hydrogen electrode (NHE). The stability of the catalysts was investigated by CV with 500 continuous voltammetric cycles at a scan rate of 50 mV s^{-1} between 0 to 1.2 V. Cyclic voltammograms for the ORR was performed by purging the electrolyte with oxygen for half an hour and then rotating the disk electrode between 100 to 2500 rpm at 5 mV s^{-1}.

HOR was evaluated before and after the potential cycling degradation test. The second potential cycling test was performed between 0.6-1.2 V with a scan rate of 20 mV s^{-1} for 1000 cycles to provide Pt dissolution/agglomeration, because in this potential region Pt metal is unstable and the oxidation/reduction cycles occur. The ESA losses for HOR were determined by comparing the activities before and after the potential cycling tests.

The data obtained from the experiments were drawn by the help of SigmaPlot11.0 and OriginPro8 programs. Electrochemical active surface area

(EASA) of Pt-based catalysts can be calculated from the data of which hydrogen adsorption and desorption peaks occur. EASA can be calculated as;

$$S_{EASA} = {Charge\ area}/{Catalyst\ Loading} \tag{3.5}$$

$$S_{EASA} = {A}/{K.L.S} \tag{3.6}$$

where A is the average area under the curves of hydrogen desorption and adsorption regions. S, is the scan rate, K ($0.21\ mC/cm^2$) is a constant and L ($28\mu g/cm^2$) is the platinum loading on glassy carbon surface per cm^2.

$$A = {(A_{adsorption} + A_{desorption})/2}\Big/{A_{glassy\ carbon}} \tag{3.7}$$

3.6.2 PEM Fuel Cell Tests

PEMFC performance tests were performed in single fuel cell hardware with a home made fuel cell test station. Before the fuel cell experiments MEAs were prepared.

3.6.2.a Preparation of Membrane Electrode Assembly

Gas Diffusion Layers (GDL) Type GDL 30 BC, SGL Carbon Germany were used for membrane electrode assembly preparation. At first, the catalyst ink consists of platinum impregnated carbon material, Nafion as a binder and 2-propanol as a solvent was prepared. This solution was held at ultrasonic bath for 30 minutes and mixing by homogenizer for 10 min. Then, this catalyst ink was sprayed onto GDLs until reaching a Pt loading of 0.4 Pt/cm^2 per electrode. Electrocatalyst Spraying unit (as shown in Figure 3.9) was used to spray the synthesized electrocatalyst ink on gas diffusion layers and to prepare electrodes.

Figure 3.9 Electrocatalyst spraying unit

After Nafion membrane were sandwiched between two electrodes, it was hot pressed at 130 °C and 250 psi for 3 min and formed a 5-layer MEA.

3.6.2.b PEM Fuel Cell Test Station

Fuel cell performance tests were performed for selected electrocatalysts in fuel cell test station built at METU Fuel Cell Research Center. The prepared electrocatalysts were used as both anode and cathode electrodes of the fuel cell where the MEAs had an active area of 2.1 x 2.1 cm^2. A single PEM fuel cell (Electrochem, FC05-01SP-REF) was used in the experiments as seen from Figure 3.10.

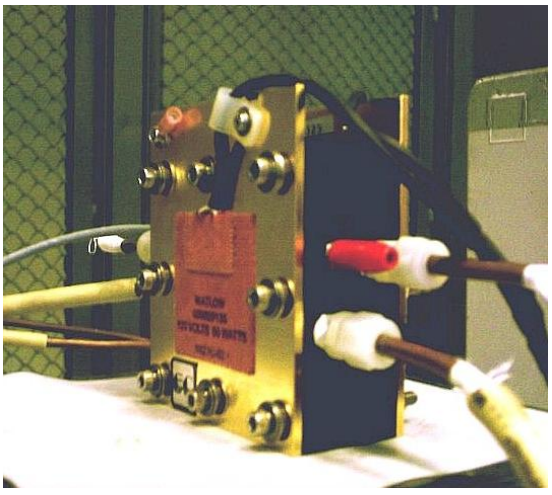

Figure 3.10 Single PEM fuel cell hardware

The fabricated power of the cell was manipulated by an electronic load (Dynaload_RBL488), which can be controlled either manually or by a computer. The software used to monitor the current and voltage responses throughout the operation was 'FCPower_ v. 2.1.102 Fideris'. To prevent the reactant gases leakage and mixing, fuel cell construction should be well sealed and compressed. If a leakage occurs, it could cause to the burning of the MEA (Bayrakçeken et al, 2008). Accordingly, silicon gaskets were used to prevent any leakage and the bolts were tightened with a torque of 1.7 Nm on each bolt. In order to prevent the condensation, the gas transfer lines between the humidifiers and the fuel cell were built with electrical-resistive-heaters (Ergün, 2009). As a result, the temperatures of the heated gas transfer lines were kept at a set temperature by on/off type temperature controllers (Erkan, 2005). The temperatures of the humidifiers were set to 70°C, and the cell temperature was set to 72°C where PID temperature controllers were used to operate the system at a required temperature. The reactant gases flow rates were adjusted as 0.1 slpm by Aalborg-171 mass flow controllers. A schematic representation of the test station is given in Figure 3.11.

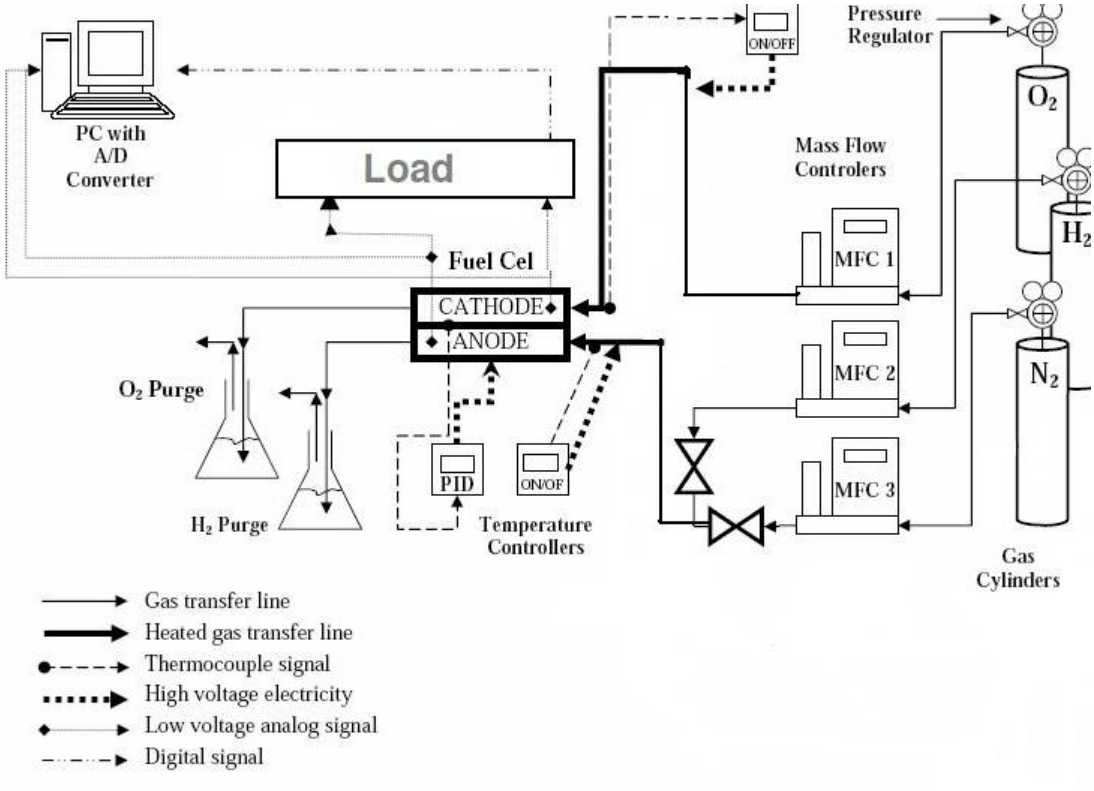

Figure 3.11 Schematic representation of fuel cell test station (modified version of Erkan, 2005)

Throughout this study, prepared electrocatalyst were tested by feeding hydrogen and oxygen gases to the system. The test procedure was as follows: after single cell was constructed with the MEA including prepared electrocatalysts, the temperatures were set to the desired values. During this time, at the anode side nitrogen was sent to the system in order to remove any oxygen from the anode electrode. After the set temperatures were reached, hydrogen and oxygen gases were fed to the system and then the cell was operated at 0.5 V until steady state. When steady state was obtained, corresponding current was measured by altering the voltage and voltage-current data named as performance curves were obtained for each electrocatalyst.

3.7 Scope of the experiments

By using different carbon precursors and different preparation conditions carbon supports having different properties were obtained. The prepared carbon

supports with different carbon precursors and experimental conditions are given in Table 3.1. According to physical characterizations one of HCMS carbon support was selected for further platinum impregnation and preparing electrocatalysts for PEM fuel cell.

Table 3.1 Carbon supports prepared with different carbon precursor and preparation conditions

Support	Template	Precursor	Synthesis Condition	Tests Performed
HCMS 1.1	SCMS-01	Phenol/paraformaldehyde	SCMS synthesized at 30°C	BET surface area, N_2 adsorption, SEM
HCMS 1.2	SCMS-02	Phenol/paraformaldehyde	SCMS synthesized at 45°C	BET surface area, N_2 adsorption
HCMS 2.1	SCMS-01	AIBN/Divinylbenzene	Molar Ratio of (DVB/AIBN)=20	BET surface area, N_2 adsorption, TEM
HCMS 2.2	SCMS-01	AIBN/Divinylbenzene	Molar Ratio of (DVB/AIBN)=24	BET surface area, N_2 adsorption
HCMS 2.3	SCMS-01	AIBN/Divinylbenzene	Molar Ratio of (DVB/AIBN)=26	BET surface area, N_2 adsorption

Selected HCMS carbon support material was used for platinum impregnation method. For platinum impregnation, different reducing agent types and amounts were used. Microwave conditions were kept constant for all experiments. Table 3.2 shows the prepared electrocatalysts by using different reducing agents and preparation conditions.

Table 3.2 Catalysts prepared with different reducing agents and preparation conditions

Sample	Carbon Support	Reducing Agent	Microwave Power	Microwave duration	Tests Performed
PtV1	Vulcan XC	EG (moderate)	800 W	2 min	TGA, XRD, PEMFC
PtV2	HCMS 2.3	EG (high)	800 W	2 min	TGA, XRD, CV
PtV3	HCMS 2.3	EG (moderate) + $NaBH_4$ (low)	800 W	2 min	TGA, XRD
PtV4	HCMS 2.3	EG (high)	800 W	2 min	TGA, XRD
PtV5	HCMS 2.3	EG (low)	800 W	2 min	TGA, XRD, CV, PEMFC
PtV6	HCMS 2.3	EG (moderate)	800 W	2 min	TGA, XRD, CV
PtV7	HCMS 2.3	EG (moderate) + Hydrazine (low)	800 W	2 min	TGA, XRD

CHAPTER 4

RESULTS AND DISCUSSION

4.1. Characterization of Solid Core Mesoporous Shell (SCMS) Silica Template

4.1.1 Porosimetric Analysis of SCMS silica template

Solid Core Mesoporous Shell (SCMS) Silica Template was synthesized with different ratios of the TEOS (silica source) and C18TMS (porogen) chemicals and the temperature of reaction medium was increased to 45°C to increase the pore size. The effects of these parameters on BET surface area, BJH method adsorption pore diameter and BJH method cumulative adsorption pore volume are given in Table 4.1 according to the sample names.

Physical properties of SCMS silica template structures are affected by changing the porogen and silica source ratios in the experiments. It was reported in the literature that the pore characteristics including the core size and shell thickness of the SCMS silica, which affect the material storage and releasing properties, can be controlled by changing the ratio of the chemicals. Controlling the structure of the SCMS allows us to control the pore diameter and surface area of the corresponding HCMS carbon supports which are very crucial parameters that affect the platinum impregnation to the structure. As can be seen from table, addition of the highest amount of TEOS (silica source) at the first stage of the synthesis (SCMS-03) resulted in a decrease in the pore diameter. On the other hand, addition of porogen (C18TMS) increased the average pore diameter of the silica structure (SCMS-04). SCMS-05

sample showed an average pore diameter in between the other values as a result of increase in the ratios of both TEOS and C18TMS at the second stage of the synthesis. In addition, surface areas of the SCMS-03, SCMS-04 and SCMS-05 samples were decreased by changing the synthesis conditions. When the temperature of the reaction medium was increased from 30°C to 45°C, the pore diameter and pore volume were decreased significantly.

Table 4.1 Comparison of BET Analysis of SCMS Silica Templates

	SCMS-01	SCMS-02	SCMS-03	SCMS-04	SCMS-05
Synthesis Parameters					
Volume Ratio of (TEOS/(TEOS+C18TMS) (mL)	6/(5+2)	6/(5+2)	10/(5+2)	6/(5+4)	6/(7+4)
Temperature Condition (°C)	30	45	30	30	30
Analysis Results					
Multipoint BET surface area (m^2/g)	444.60	555.50	435.10	289.70	203.80
BJH Method Average Adsorption Pore Diameter(nm)	2.55	2.20	2.45	2.62	2.51
BJH Method Cumulative Adsorption Pore Volume (cm^3/g)	0.41	0.27	0.35	0.24	0.18

SCMS-01 sample was selected in order to synthesize the corresponding HCMS carbon support due to its largest pore volume and high surface area. N_2 adsorption/desorption isotherms and pore size distribution of the SCMS-01 silica template are given in Figure 4.1 and Figure 4.2, respectively. N_2 adsorption/desorption analysis was conducted at 77 K. Brauner-Emett-Teller (BET)

surface area of SCMS-01 silica was calculated as 444.6 m^2/g for a total pore volume of 0.41 cm^3/g.

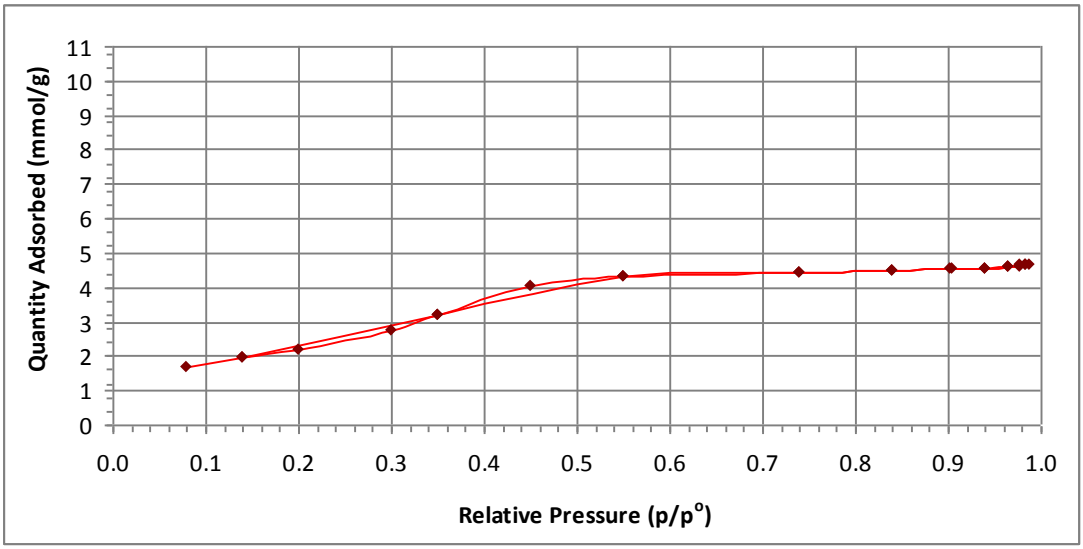

Figure 4.1 N_2 adsorption/desorption isotherm of SCMS-01 silica template

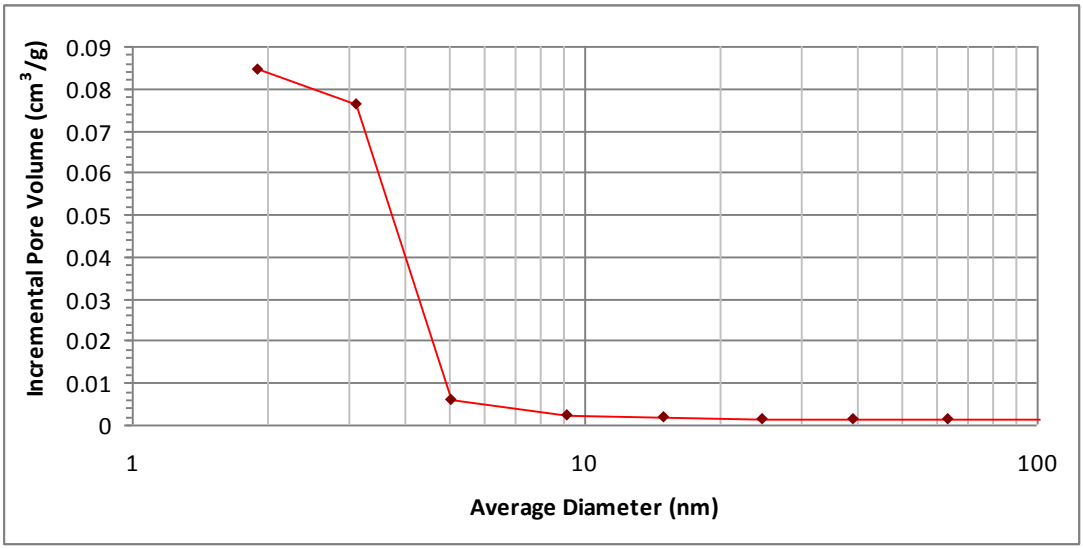

Figure 4.2 Pore Size Distribution of SCMS-01 silica template

Corresponding pore size distribution data for SCMS-01 silica template were calculated from the nitrogen isotherms' adsorption branches by the Barrett–Joyner–Halenda (BJH) method which showed that the pores are uniform with narrow pore size distribution centered at 2.55 nm.

4.1.2 Characterization of SCMS silica template by Energy Dispersive X-Ray Spectroscopy (EDXS)

Energy Dispersive X-Ray Spectroscopy analysis was performed for one of the samples in order to determine the composition of the surface elements and given in Figure 4.3. Au atoms present in the analysis resulted due to the coating of the sample with a very thin layer of gold by a machine called a sputter coater to make it conductive. Thus, it can be seen from Figure 4.3 and Table 4.2 that the content includes only silica and oxygen atoms as expected from the SiO_2 formation for the SCMS silica templates.

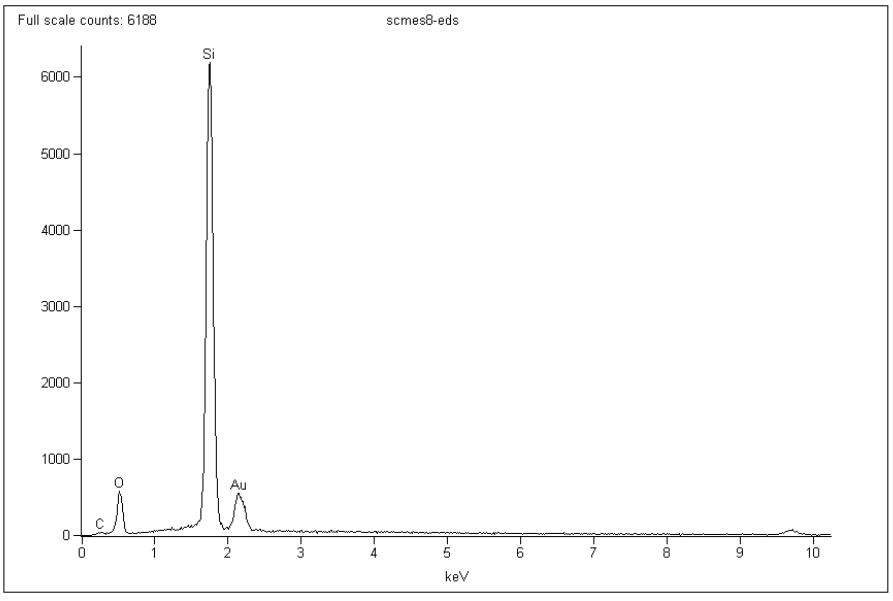

Figure 4.3 Energy Dispersive X-Ray Analysis Result as Percentages for SCMS Sample

Table 4.2 Energy Dispersive X-Ray Analysis Result as Percentages for SCMS Sample

Element	Weight Conc %	Atom Conc %
O	37.57	58.93
Si	43.24	38.63
Au	19.19	2.44

4.1.3 Characterization of SCMS silica template by Thermal Gravimetric Analysis (TGA)

The thermal behavior of SCMS-01 silica template was investigated by thermal gravimetric analysis (TGA) as given in Figure 4.4. As can be seen from figure that the organic groups could be removed from the SCMS silica structure after 256 ºC and calcination process was completed at 600 ºC. After that temperature, stabilization occurred and silica present into the material even at the high temperatures. TGA result confirmed that performing calcination process for the SCMS silica synthesis at 550 ºC under oxygen flow is appropriate.

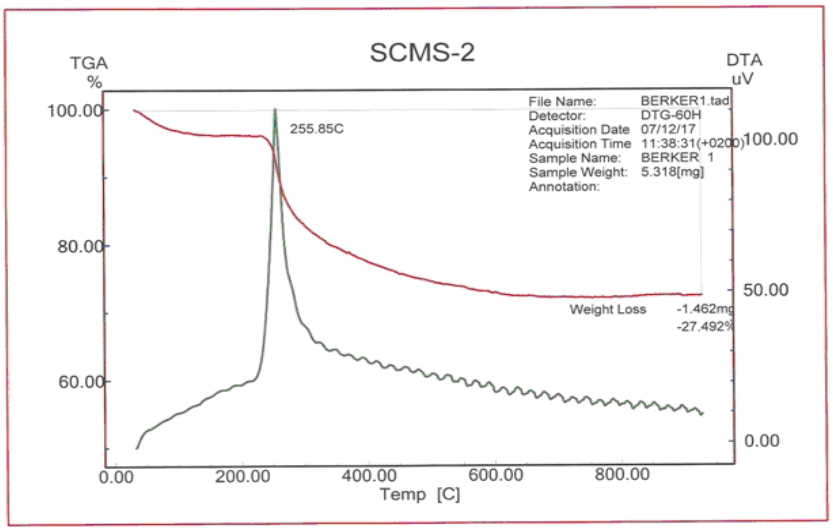

Figure 4.4 TGA analysis of SCMS-01

4.1.4 Characterization of SCMS silica template by Scanning Electron Microscopy (SEM)

The surface morphology of the SCMS-01 silica template was investigated by scanning electron microscopy (SEM) with a magnification range from 15x to 200,000x (reached in 25 steps) and a resolution of 5 nanometers. SEM image of SCMS silica template is given in Figure 4.5 As can be seen from figure that most of the particles are uniform and spherical with particle diameters of approximately 500 nm.

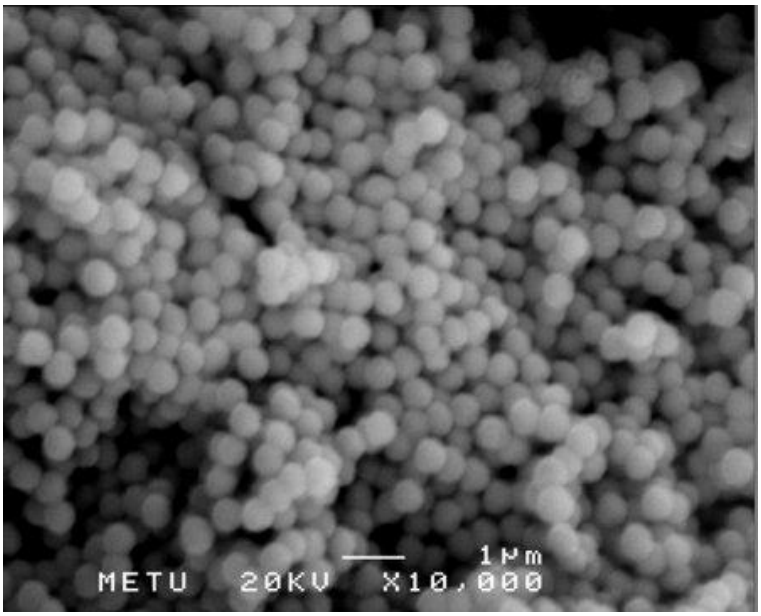

Figure 4.5 SEM image of SCMS-01 silica template

4.2. Characterization of Hollow Core Mesoporous Shell (HCMS) Carbon Support

4.2.1 Porosimetric Analysis of HCMS carbon support

HCMS carbon support synthesis was carried out by two different routes. In the first (1^{st}) route, phenol and paraformaldehyde were used as the carbon source. SCMS-01 and SCMS-02 samples were used as the silica templates for carbon

synthesis via 1st route, and it was observed that BJH adsorption pore diameter was 1.05 and 1.47 nm, respectively. To increase the pore sizes of carbon support further, second (2nd) route carbon support synthesis was conducted using divinylbenzene (DVB) as the carbon source. In the 2nd route synthesis the molar ratios of the carbon source (DVB) to Azobisisobutyronitrile (AIBN) were changed as 20, 24 and 26. The structural properties of the synthesized HCMS carbon supports via 1st and 2nd routes are given in Table 4.3.

Table 4.3 Structural Properties of HCMS Carbon Supports

	HCMS 1.1	HCMS1.2	HCMS 2.1	HCMS 2.2	HCMS 2.3
Synthesis Parameters					
Synthesis Routes	(1st route)	(1st route)	(2nd route)	(2nd route)	(2nd route)
Silica Template Type	SCMS-01	SCMS-02	SCMS-01	SCMS-01	SCMS-01
Molar Ratio of (DVB/AIBN)			20	24	26
Analysis Results					
Multipoint BET surface area (m^2/g)	1053	1034	1182	1072	852
BJH Method Average Adsorption Pore Diameter (nm)	1.05	1.47	3.07	3.41	3.44
BJH Method Cumulative Adsorption Pore Volume (cm^3/g)	$4.94x10^{-1}$	$5.53x10^{-1}$	1.88	1.50	1.37

Table 4.3 showed that following the 2nd route carbon synthesis with a molar ratio of DVB/AIBN=26 resulted in a BJH adsorption pore diameter of 3.44 nm for HCMS 2.3. Table 4.3 also revealed that increasing the molar ratio of DVB/AIBN had a positive effect on the increase of the pore diameter. When the same silica template used, it was seen that 2nd synthesis route gave larger pore diameters when compared to 1st synthesis route. Because of the higher pore diameter, HCMS 2.3 carbon support was selected for further studies including platinum impregnation via microwave irradiation method.

N_2 adsorption/desorption isotherms and pore size distribution of the HCMS 2.3 are given in Figure 4.6 and Figure 4.7, respectively. Brauner-Emett-Teller (BET) surface area of HCMS 2.3 was calculated as 852 m^2/g for a total pore volume of 1.37 cm^3/g. Corresponding pore size distribution data for HCMS-2.3 carbon support calculated from the adsorption branches of nitrogen isotherms by the BJH method showed that the pores are uniform with narrow pore size distribution centered at 3.44 nm.

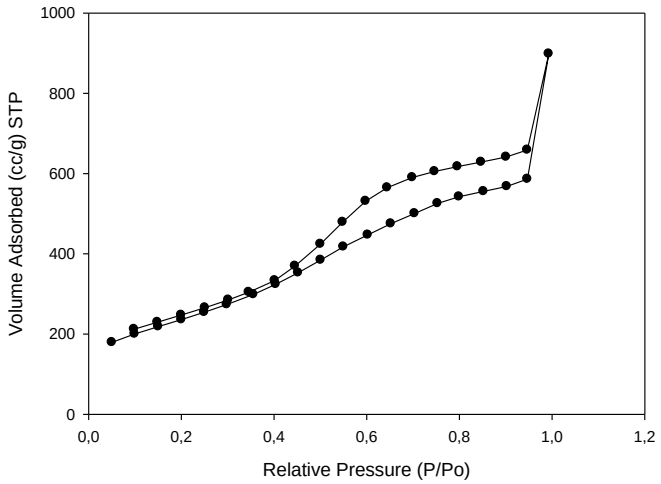

Figure 4.6 N_2 adsorption/ desorption isotherm for HCMS 2.3 carbon support

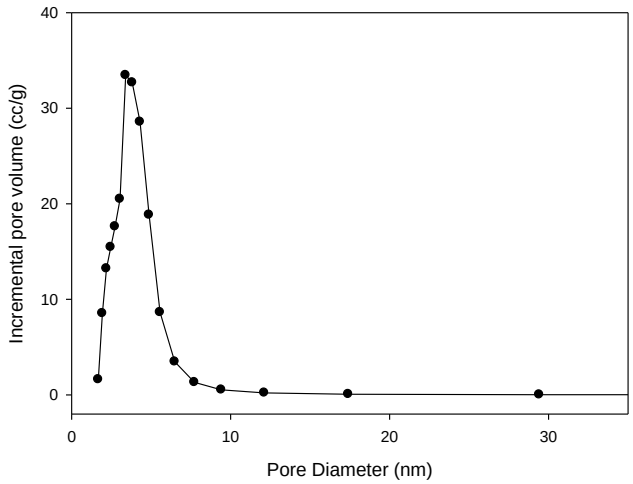

Figure 4.7 Pore size distribution for HCMS 2.3 carbon support

4.2.2 Characterization of HCMS carbon support by TGA

TGA analysis was also performed to HCMS 2.3 as given in Figure 4.8. As seen from Figure 4.8, calcination process for the HCMS carbon material exhibited stability. The process was performed in two stages; firstly the temperature was raised to 160 ºC and waited for 5 h at this temperature and then it was raised to 850 ºC and waited here for 7 h. According to TGA result, calcination process was appropriate for these temperature ranges.

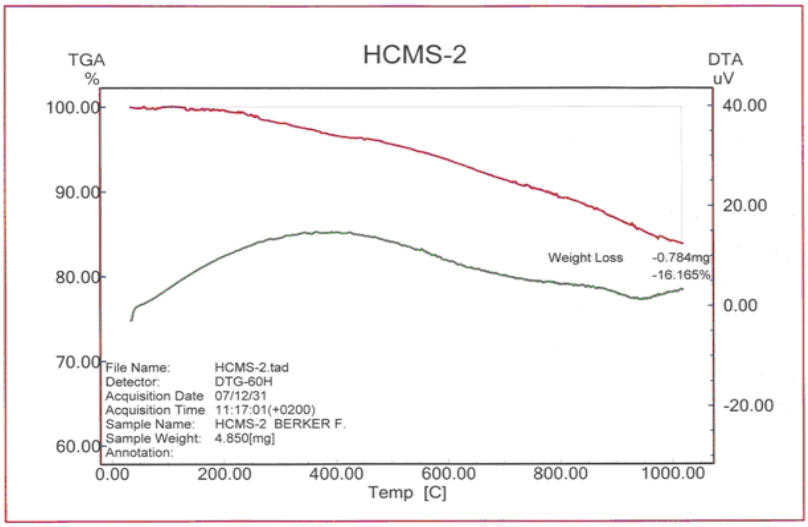

Figure 4.8 TGA analysis of HCMS carbon support

4.2.3 Characterization of HCMS carbon support by Transmission Electron Microscopy (TEM)

TEM image of HCMS carbon support is given in Figure 4.9 (Fıçıcılar, 2009). The same HCMS carbon support material was used in this study to increase the platinum weight percentage on carbon material. In the image, particles of HCMS carbon support exhibited a uniform particle size. It was calculated that HCMS carbon's core diameter was 340 nm and shell thickness was 80 nm.

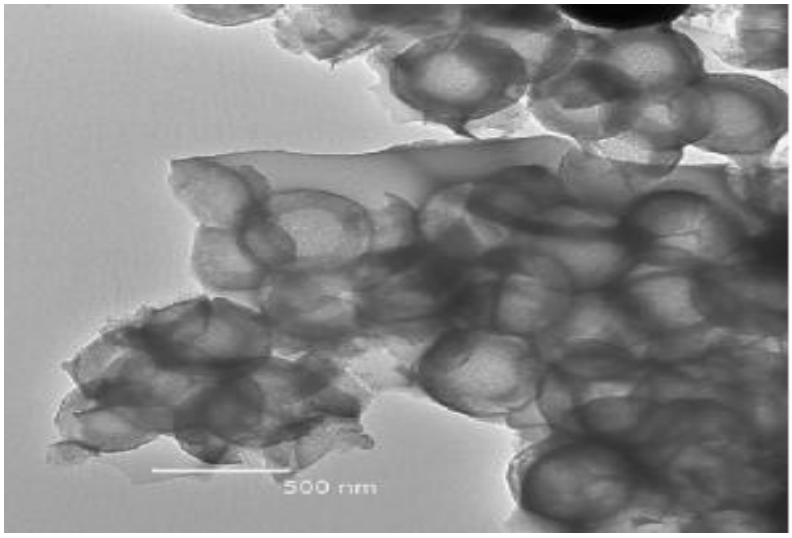

Figure 4.9 TEM image of hollow core mesoporous shell (HCMS) carbon

4.3. Catalyst Preparation via Microwave Irradiation

Platinum (Pt) impregnation was conducted by microwave irradiation method. Reducing agents used in the experiments were ethylene glycol, hydrazine and sodium borohydride. The required thermal environment for the reduction of platinum particles on carbon support was supplied by microwave oven. Microwave conditions were set to 800 Watts and 2 min for all experiments. A commercially available carbon support, Vulcan XC, and commercial catalyst, 20% Pt/C (ETEK), were also used for comparison.

4.3.1 Characterization of Pt based catalysts by TGA

TGA experiments were performed under the flowing air to roughly estimate the Pt content. The corresponding TGA results are given in Figures 4.10- 4.16.

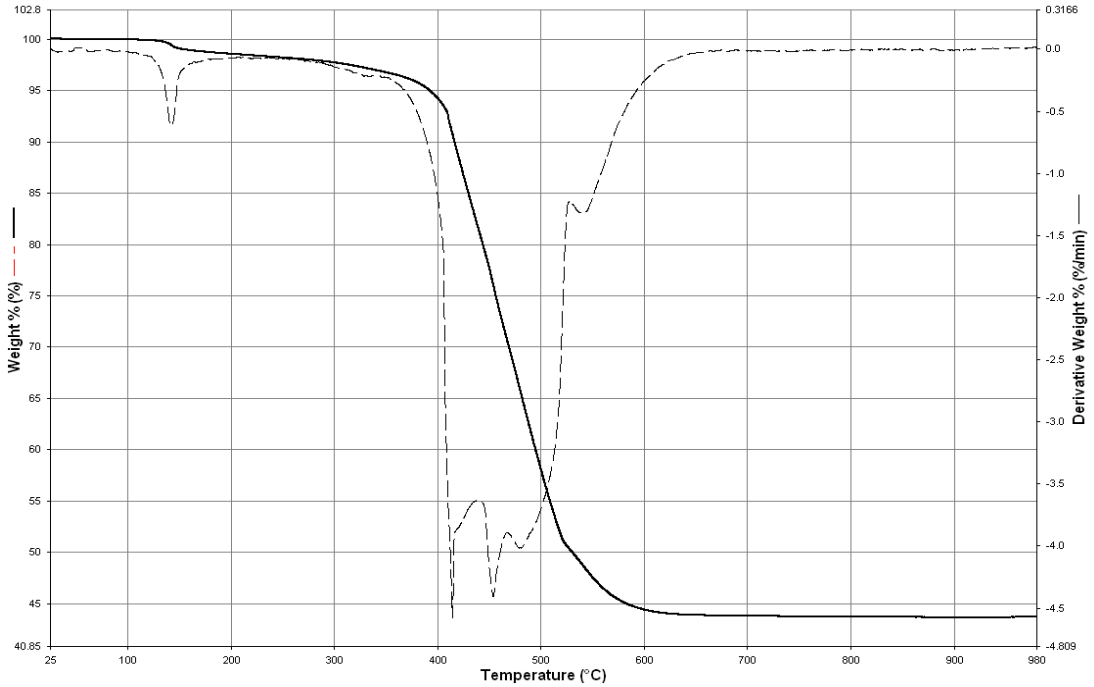

Figure 4.10 TGA result of 44 % Pt/Vulcan XC catalyst

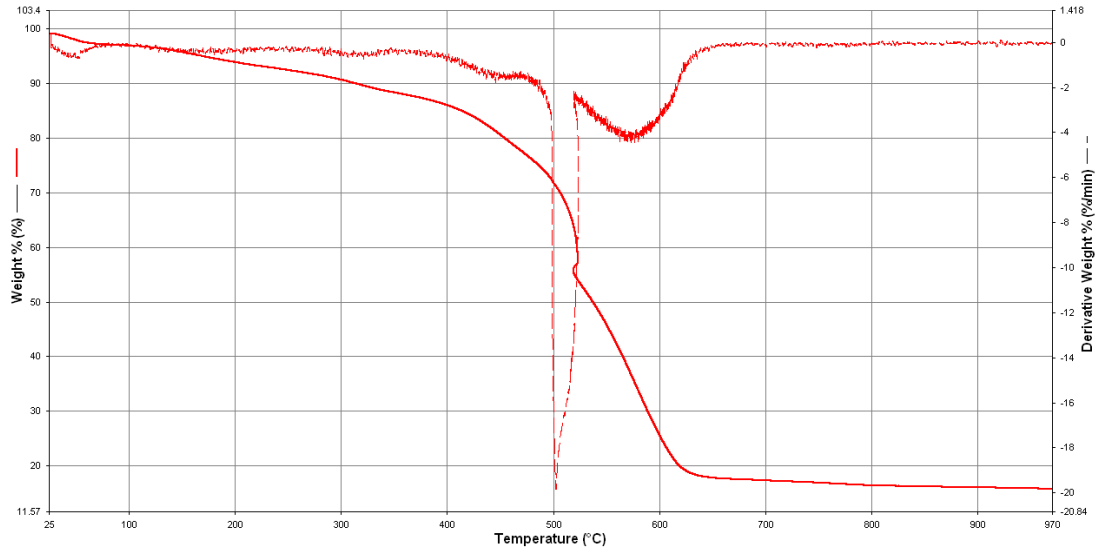

Figure 4.11 TGA result of 17 % Pt/HCMS catalyst

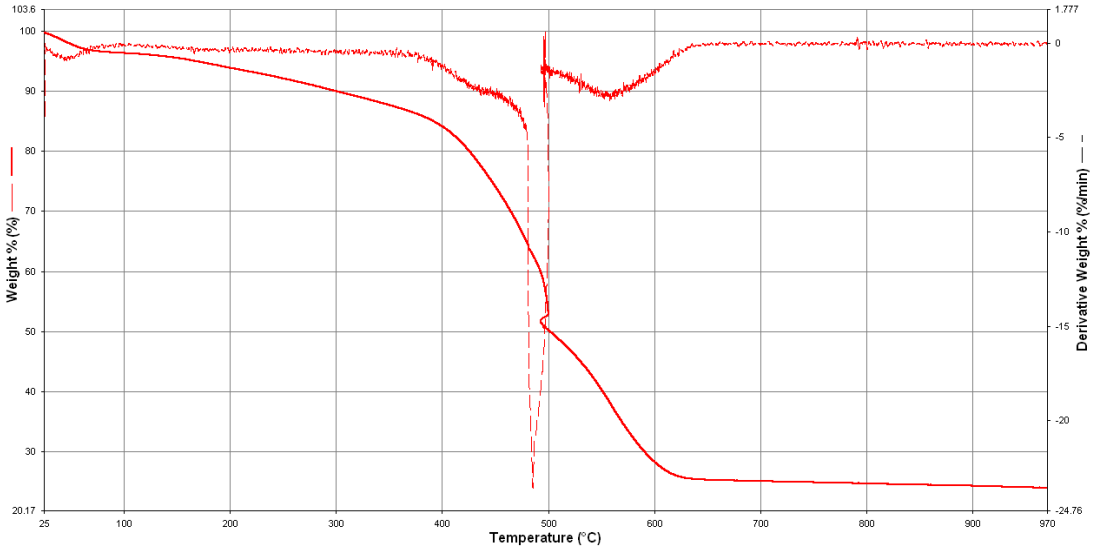

Figure 4.12 TGA result of 23 % Pt/HCMS catalyst

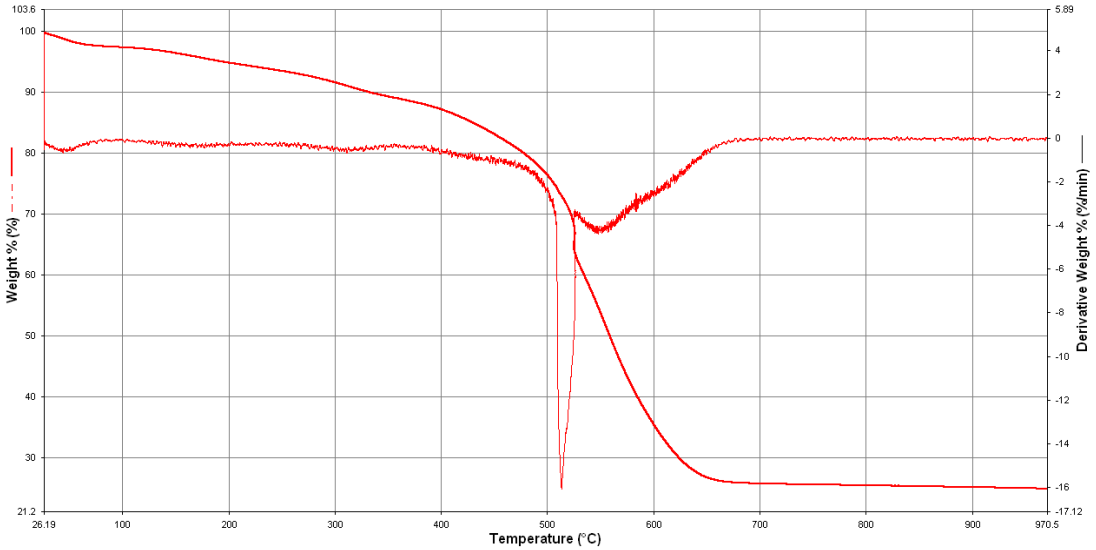

Figure 4.13 TGA result of 24 % Pt/HCMS catalyst

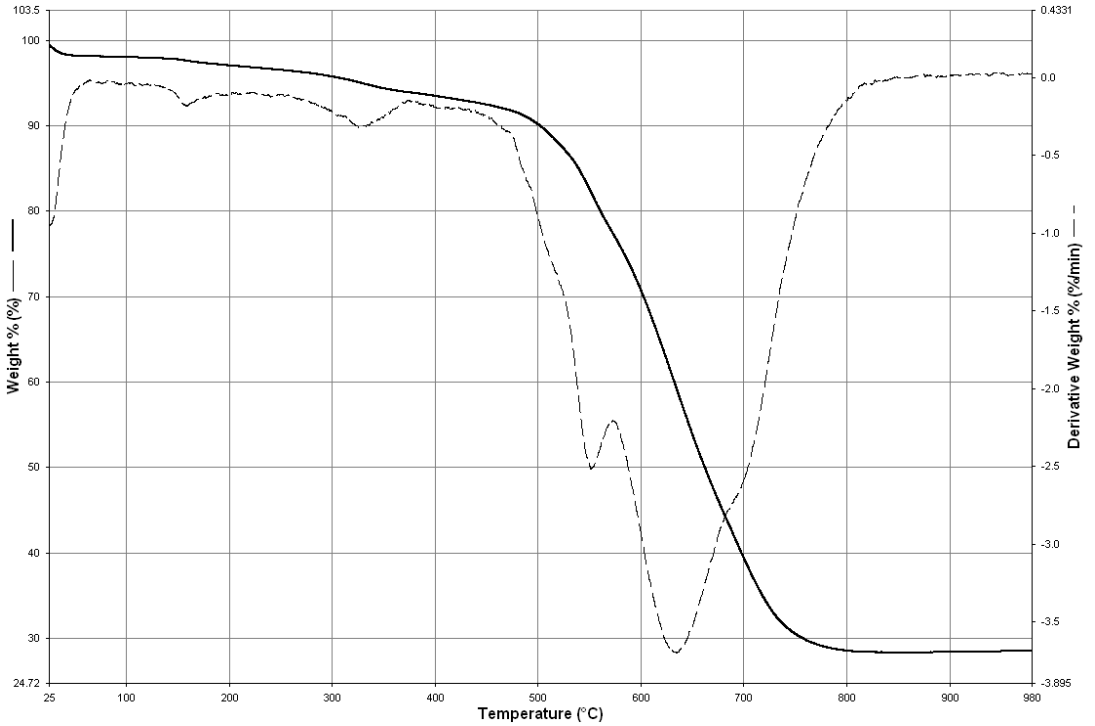

Figure 4.14 TGA result of 28 % Pt/HCMS catalyst

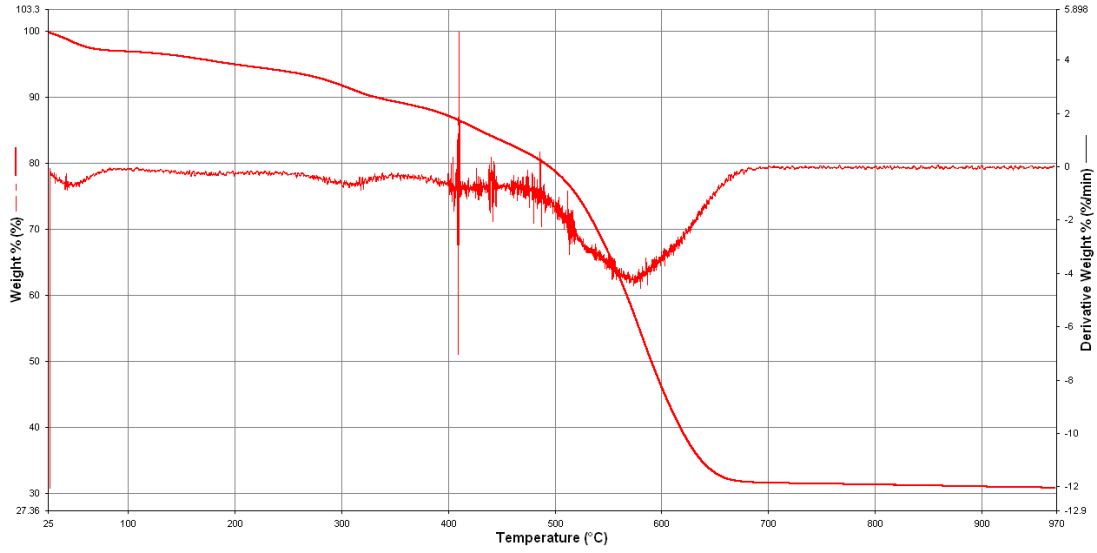

Figure 4.15 TGA result of 31 % Pt/HCMS catalyst

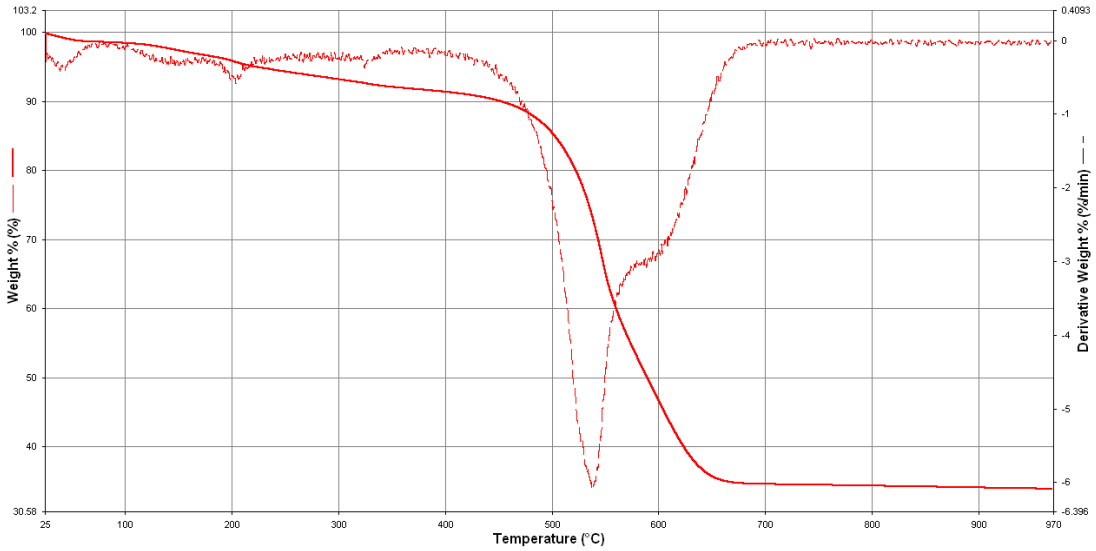

Figure 4.16 TGA result of 34 % Pt/HCMS catalyst

The Pt weight percentages obtained from the TGA results summarized in Table 4.4 for different catalyst preparation conditions. As seen from Table 4.4, TGA analysis results shows that 44% Pt impregnation was achieved for commercial carbon support named as Vulcan XC by using moderate amount of ethylene glycol. For the impregnation of synthesized carbon supports, utilization of moderate amount of ethylene glycol resulted in 28% Pt/HCMS 2.3 electrocatalyst. Increase in the ethylene glycol amount did not cause an increase in the weight percentage of platinum on carbon support. $NaBH_4$ usage as an additional reducing agent did not increased the loading significantly also. If the moderate amount of ethylene glycol was used with an additional reducing agent of hydrazine, the Pt loading was increased up to 34% for PtV5 sample.

Table 4.4 Comparison of TGA analysis results of Platinum impregnated catalysts

Sample	Reducing Agent	Microwave Power	Microwave duration	TGA result Pt wt %
(Pt/ Vulcan XC)				
PtV1	EG (moderate)	800 W	2 min	44%
(Pt/HCMS 2.3)				
PtV2	EG (high)	800 W	2 min	17 %
PtV3	EG (moderate) + $NaBH_4$ (low)	800 W	2 min	23%
PtV4	EG (high)	800 W	(2+1) min	24%
PtV5	EG (low)	800 W	2 min	28%
PtV6	EG (moderate)	800 W	2 min	32%
PtV7	EG (moderate) + hydrazine (low)	800 W	2 min	34%

4.3.2 Characterization of Pt based catalysts by XRD

Prepared electrocatalysts were also characterized by XRD and the corresponding particle sizes were calculated by using the XRD data and Scherrer formula by using the peak located at (220) inflection. XRD results are given in Figure 4.17. Characteristic peaks that correspond to the face-cubic-centered (fcc) Pt were obtained for all catalysts as (111), (200) and (220). Sharpening of the peaks indicates that the particle size of the catalysts is getting larger. Corresponding particle sizes of the catalysts are given in Table 4.5.

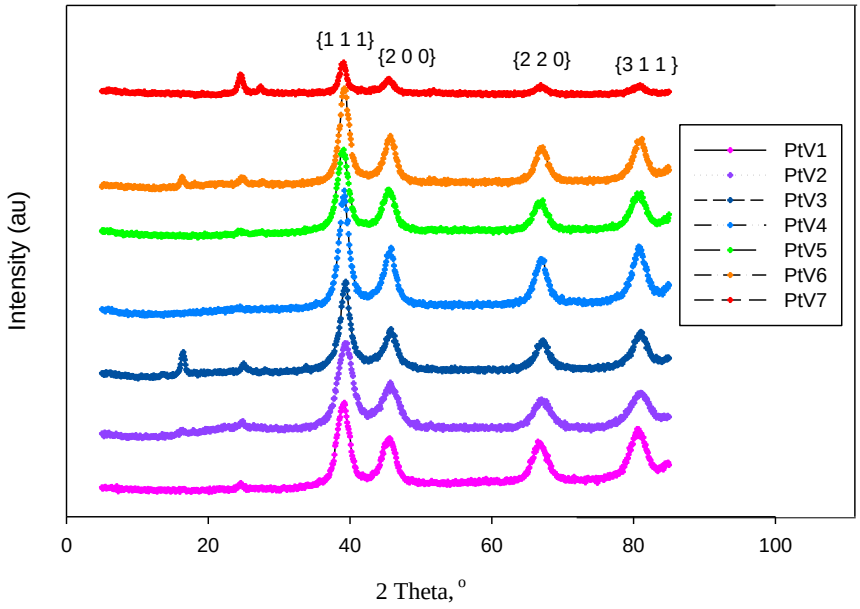

Figure 4.17 XRD results for the prepared catalysts

Ethylene glycol (EG) was used as the solvent and reducing agent. Table 4.5 shows that addition of another reducing agent nearby EG caused the particle sizes to increase. Addition of $NaBH_4$ did not have any improvement effect on the properties of the catalysts according to their Pt wt % and particle size. Addition of hydrazine nearby EG resulted in a higher Pt loading over the carbon support but this time the highest particle size was obtained. It was observed that the catalyst properties including particle size and Pt loading strongly affected by the catalyst preparation conditions.

Table 4.5 Comparison of XRD analysis results of Platinum impregnated catalysts

Sample	Reducing Agent	Pt wt %	Microwave duration	Particle size (nm)
(Pt/ Vulcan XC)				
PtV1	EG (moderate)	44%	2 min	3.4
(Pt/HCMS 2.3)				
PtV2	EG (high)	17 %	2 min	3.2
PtV3	EG (moderate) + $NaBH_4$ (low)	23%	2 min	4.2
PtV4	EG (high)	24%	(2+1) min	4.2
PtV5	EG (low)	28%	2 min	4
PtV6	EG (moderate)	32%	2 min	4.2
PtV7	EG (moderate) + hydrazine (low)	34%	2 min	4.5

4.4 Cyclic Voltammetry Tests

Cyclic voltammetry is a useful electrochemical tool in order to determine the electrochemical activity of the catalysts in a fast way and by using less amount of material. It can also be used to determine the double layer capacitance and corrosion of the carbon materials.

4.4.1 HCMS Carbon Support Corrosion Test

Thermodynamically carbon can be oxidized to carbon dioxide above 0.207 V versus NHE as follows:

$$C + 2H_2O \rightarrow CO_2 + 4H^+ + 4e^- \qquad E=0.207\ V \qquad (4.1)$$

Oxidation of carbon support is called carbon corrosion and can decrease the performance losses in the fuel cell due to the accelerated loss of active surface area and the change in the pore morphology and pore surface characteristics (Maass et al., 2008).

The electrochemical oxidation of the synthesized HCMS carbon support was investigated by continous potential cycling and potential holding tests. Continuous potential cycling was conducted up to 500 cycles with a scan rate of 50 mV/s and given in Figure 4.18. It was seen that there was an obvious current peak appears approximately 0.55 V which is believed that resulted from the surface oxide formation due to the hydroquinone-quinone (HQ-Q) redox couple on the carbon black support surface. At low cycle numbers the current peak is also seen which may indicate that the synthesized carbon supports also have some surface oxide groups on the surface after the synthesis. As the number of cycles increase the peak becomes more pronounced which means that the carbon oxidation over the carbon support surface also increases.

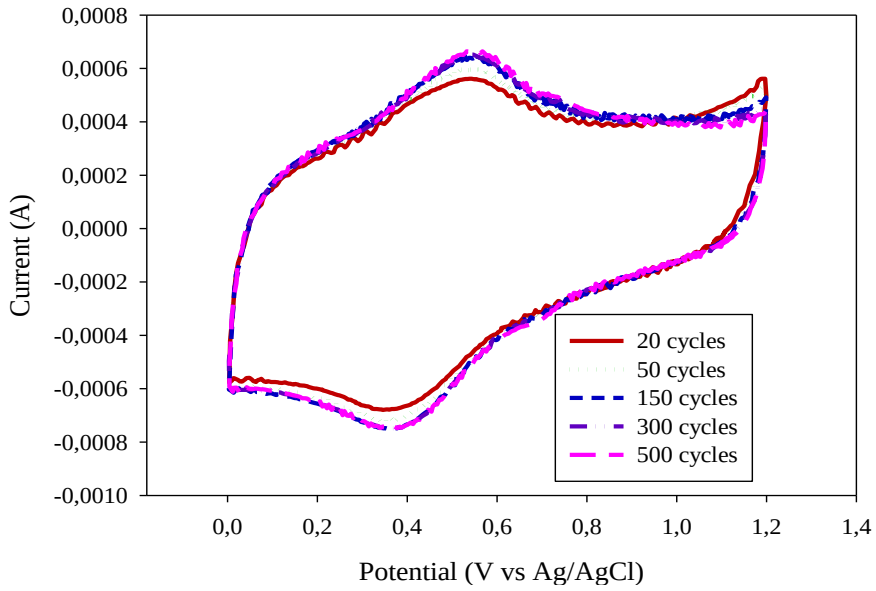

Figure 4.18 Cyclic voltammograms for HCMS 2.3 carbon support after potential cycling up to 500 cycles in 0.1 M $HClO_4$ with a scan rate of 50 mV/s

4.4.2 Effect of Pt Loading on HOR Activity of HCMS Supported Pt Catalysts

To examine the effect of platinum loading on the hydrogen oxidation reaction activity of the electrocatalysts half cell CV tests were conducted for 17, 28 and 32 wt % Pt/HCMS 2.3 electrocatalysts. The cyclic voltammograms for these electrocatalysts up to 500 cycles are given in Figure 4.19. As can be seen from figure, the double layer capacitance of the electrocatalysts decreases as the Pt loading increases. The principle of double layer capacitance at the electrode/electrolyte interface is the accumulation of the electric charges on the electrode surface while ions of opposite charge are arranged in the electrolyte side. Double layer capacitance depends critically on surface area of carbon material used in electrodes. The higher the specific surface area of the carbon means the higher the specific capacitance. In addition, carbon materials with larger pores should be capable of delivering high power because it can be discharged/ charged at higher current density because larger pores would provide more favorable and quicker pathway for ions to penetrate (Xing et al., 2006). Since 17 wt% Pt/HCMS has the highest specific surface area because of low Pt loading and the lowest particle size with 3.2 nm, its capacitance is the highest one when compared to other high Pt loading electrocatalysts. An the same time, 32 wt % Pt/HCMS exhibited the lowest doucle layer capacitance effect having the largest particle size of 4.2 nm and lowest specific surface area. In addition, electrochemical active surface areas of 17, 28 and 32 wt % Pt/HCMS catalysts after 500 cycles in 0.1 M $HClO_4$ with a scan rate of 50 mV/s were also calculated and given in Table 4.6. 28 wt % Pt/HCMS 2.3 catalyst showed the highest ESA as 2.992 m^2/g.

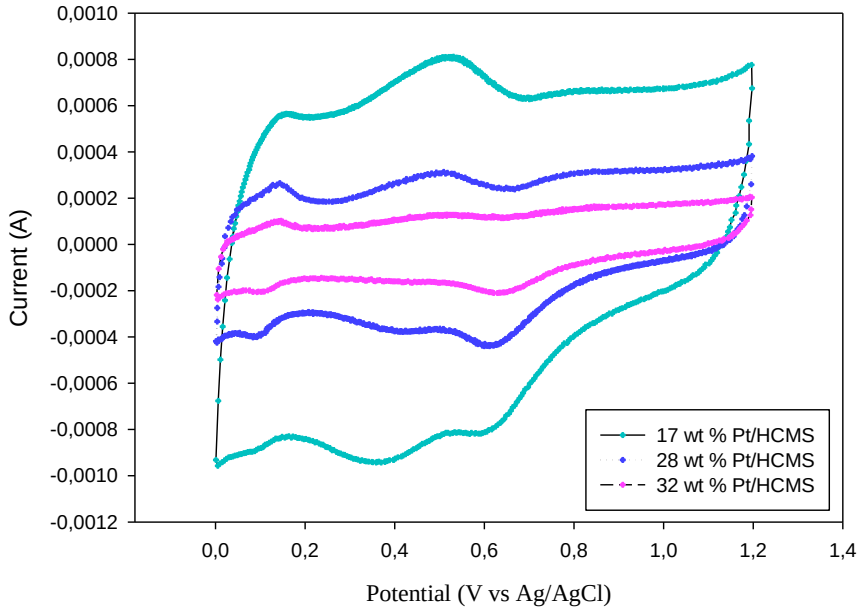

Figure 4.19 Cyclic voltammograms of 17, 28 and 32 wt % Pt/HCMS for HOR after 500 cycles in 0.1 M $HClO_4$ with a scan rate of 50 mV/s

Table 4.6 Comparison of Electrochemical Active Surface Areas of 17, 28 and 32 wt % Pt/HCMS for HOR after 500 cycles in 0.1 M $HClO_4$ with a scan rate of 50 mV/s

Catalyst Type	17 wt % Pt/HCMS	28 wt % Pt/HCMS	32 wt % Pt/HCMS
ESA for hydrogen desorption peak (m^2/g)	0.077	0.794	0.525
ESA for hydrogen adsorption peak (m^2/g)	1.372	2.198	1.428
Total ESA (m^2/g)	1.449	2.992	1.953

The stability of the high Pt loading electrocatalysts was investigated by continuous potential cycling. Figure 4.20 shows the effect of potential cycling up to 500 cycles on the HOR activity of the 28% Pt/HCMS2.3 electrocatalyst. The

hydrogen adsorption/desorption peaks were obviously seen and they used for the calculation of the electrochemical active surface area with the help of ORIGIN software by taking the average of the areas under the curve under hydrogen adsorption/desorption peak. Active electrochemical surface areas (ESAs) of the prepared 28 wt % Pt/HCMS 2.3 electrocatalyst were calculated as 13.3 m^2/g Pt and 9.5 m^2/g Pt after 20 and 500 cycles, respectively. ESA was decreased about 29% after potential cycling which may be attributed to both carbon corrosion and Pt agglomeration and dissolution.

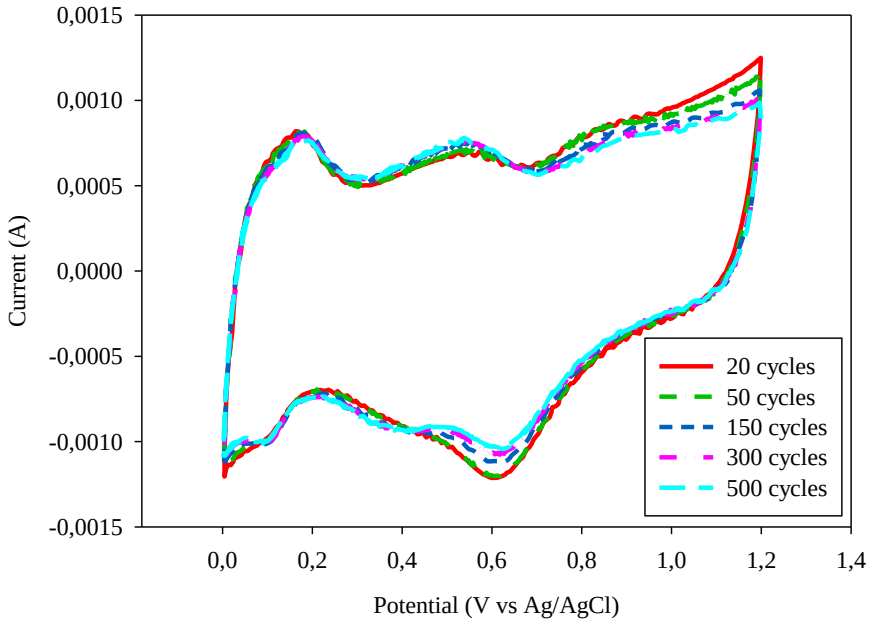

Figure 4.20 Cyclic voltammogram of 28 wt % Pt /HCMS 2.3 electrocatalsyst during continuous potential cycling in 0.1 M $HClO_4$ with a scan rate of 50 mV/s

In 20 and 50 cycles, the HCMS oxide reduction peak appeared as a shoulder but further increase in the number of cycles (150 to 500) resulted in a clearly distinguished second peak in addition to the Pt oxide reduction peak. This observation is in agreement with the studies in the literature where these peaks are attributed to oxidation and reduction reactions of surface oxygen groups attached to carbon (Panić et al., 2008). As the number of cycles increased, the intensity of the

peaks corresponding to carbon oxidation/reduction also increased. There was a positive shift of the platinum oxide reduction peaks during the potential cycling.

The cyclic voltammograms of 32 wt % Pt/HCMS electrocatalyst which has the highest Pt loading are given in Figure 4.21. The voltammograms were cycled up to 1500 cycles with a scan rate of 50 mV/s. As can be seen from figure, ESA also decreases as the number of cycle increases. Electrochemical Active Surface Areas (ESAs) of each cycle were calculated and given in Table 4.7.

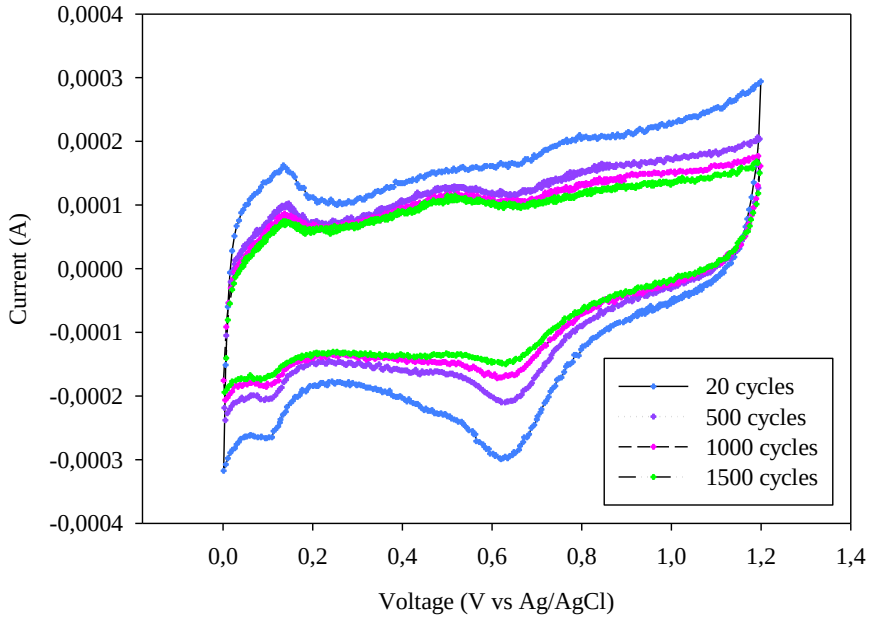

Figure 4.21 Cyclic voltammogram of 32 wt % Pt /HCMS 2.3 electrocatalsyst during continuous potential cycling in 0.1 M $HClO_4$ with a scan rate of 50 mV/s

Table 4.7 Comparison of Electrochemical Active Surface Area of 32 wt %Pt/HCMS electrocatalysts for different cycles

Number of cycles	20	500	1000	1500
ESA (m^2/g)	3.117	1.953	1.336	1.208
% ESA loss In comparison with 20 cycles	-	37.344	57.138	61.245

Another accelerated degredation test (ADT) was also performed to 28 wt % Pt/HCMS 2.3 electrocatalyst including the potential cycling between 0.6-1.2 V (in which Pt oxidation/reduction occurs and Pt is unstable) up to 1000 cycles with a scan rate of 20 mV/s. Figure 4.22 represents the cyclic voltammogram for 28% Pt/HCMS 2.3 electrocatalyst before and after ADT. It was observed that the ESA also decreases during ADT and carbon oxide peaks are getting more pronounced. ESA was calculated as 5.726 and 3.676 m^2/g before and after ADT, respectively. ADT was resulted in an ESA loss of 35.8 % which can be attributed to the agglomeration of the small particles ans also the carbon corrosion.

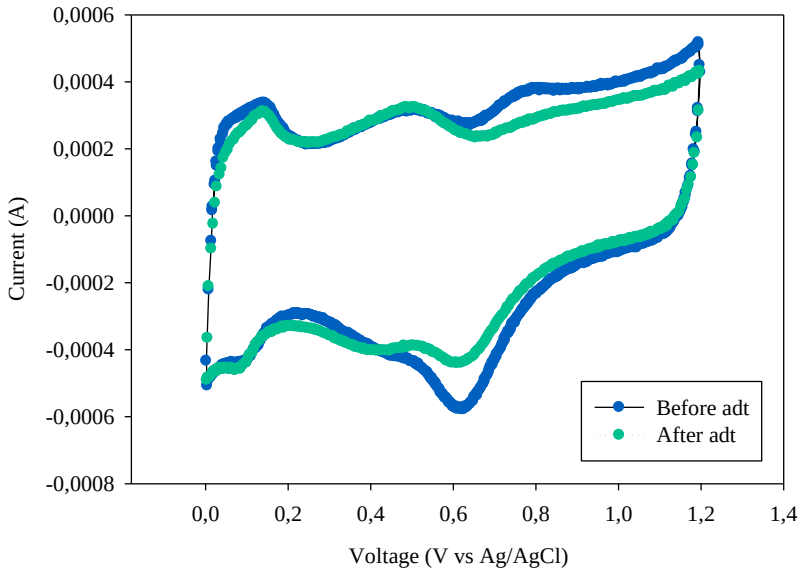

Figure 4.22 Cyclic voltammogram of 28 wt % Pt /HCMS 2.3 electrocatalsyst before and after ADT in 0.1 M $HClO_4$ with a scan rate of 50 mV/s

4.4.3 Effect of Pt Loading on ORR Activity of HCMS Supported Pt Catalysts

ORR activity of the prepared 28 and 32 wt % Pt/HCMS electrocatalysts were also investigated and given in Figures 4.23 and 4.24, respectively. ORR data were obtained by purging the electrolyte with oxygen half an hour and then rotating the disk electrode between 100-2500 rpm with a scan rate of 5 mV/s in 0.1 M $HClO_4$.

The ORR activity of the catalysts can be examined by measuring the current at 0.9 V (vs NHE) and then dividing this current by Pt mass in order to obtain the so-called mass activity ($i_{m(0.9\ V)}$, A/mg_{Pt}) or by the electrochemically active Pt surface area to obtain specific activity ($i_{s(0.9\ V)}$, $\mu A/cm^2_{Pt}$) as given with the following equation where mass and specific activities can be related via the Pt specific surface area (A_{Pt}) (Chen et al., 2010).

$$i_m(0.9\ V)\ (A/mg_{Pt}) = i_{s(0.9\ V)}\ (\mu A/cm^2_{Pt}) \times A_{Pt}(m^2_{Pt}/g_{Pt}) \times 10^{-5} \qquad (4.2)$$

By using the data obtained from Figures 4.23 and 4.24 and Equation 4.2 corresponding mass activities for the 28 and 32 % Pt/HCMS catalysts were calculated as 125 and 85.3 mA/ mg_{Pt}, respectively, at 1600 rpm rotation speed. This result shows that 28 % Pt/HCMS had a better ORR activity than 32 % Pt/HCMS which can be attributed to higher electrochemical surface area which could be caused by high dispersion and uniform distribution of the Pt particles on the HCMS carbon support (Song et al., 2007).

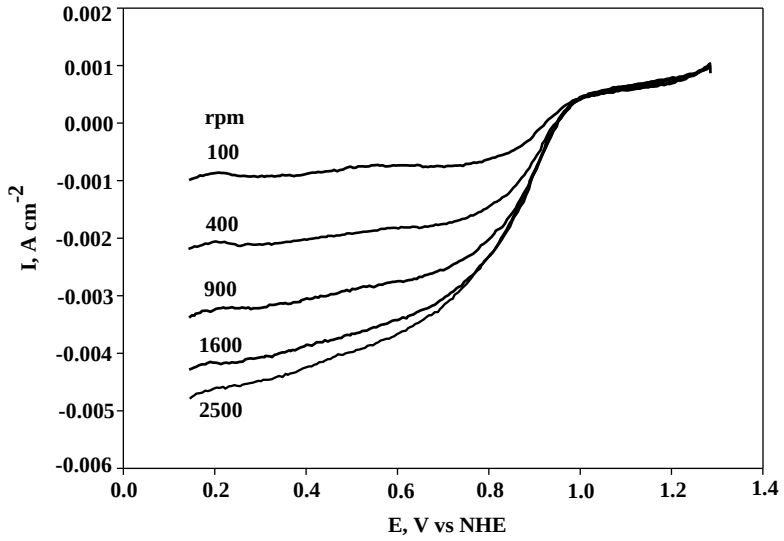

Figure 4.23 Hydrodynamic voltammograms of positive scan of Pt/HCMS (28%) for oxygen reduction in O_2 saturated 0.1 M $HClO_4$ with a scan rate of 5 mV/s

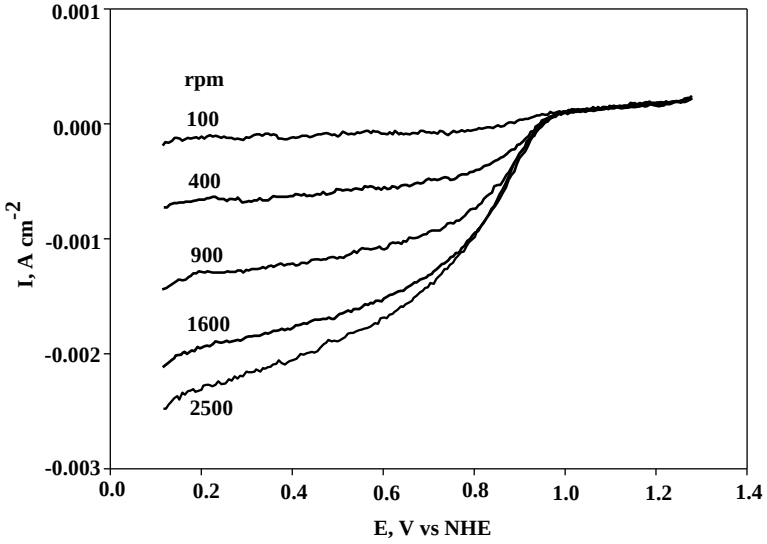

Figure 4.24 Hydrodynamic voltammograms of positive scan of Pt/HCMS (32%) for oxygen reduction in O_2 saturated 0.1 M $HClO_4$ with a scan rate of 5 mV/s

4.5. Results of Fuel Cell Performance Tests

PEM fuel cell tests were also performed to determine the electrocatalytic activity of the prepared catalysts in the fuel cell environment. Figures 4.25 and 4.26 show the fuel cell performances of the cells prepared with different anode and cathode electrocatalysts based on different carbon supports. Figure 4.25 showed the effect of increase in Pt loading on the performance of PEM fuel cell when the commercial Vulcan XC carbon support was used as the electrocatalyst support. Two different fuel cells were constructed. One of them was prepared with the 44% Pt/Vulcan XC as both anode and cathode electrocatalysts. Other fuel cell was constructed with commercial 20% Pt/C (ETEK) catalyst as the anode and 20% Pt/Vulcan XC prepared by microwave irradiation as the cathode. For each electrode, Pt loading was set to 0.4 mg Pt/cm^2. Figure 4.25 revealed that increase in the Pt weight percentages on carbon support resulted in an increase on the PEM fuel cell

performance. The increase in the Pt amount over the carbon support may enhance the contact of the catalyst with the electrolyte and also it may decrease the contact resistance.

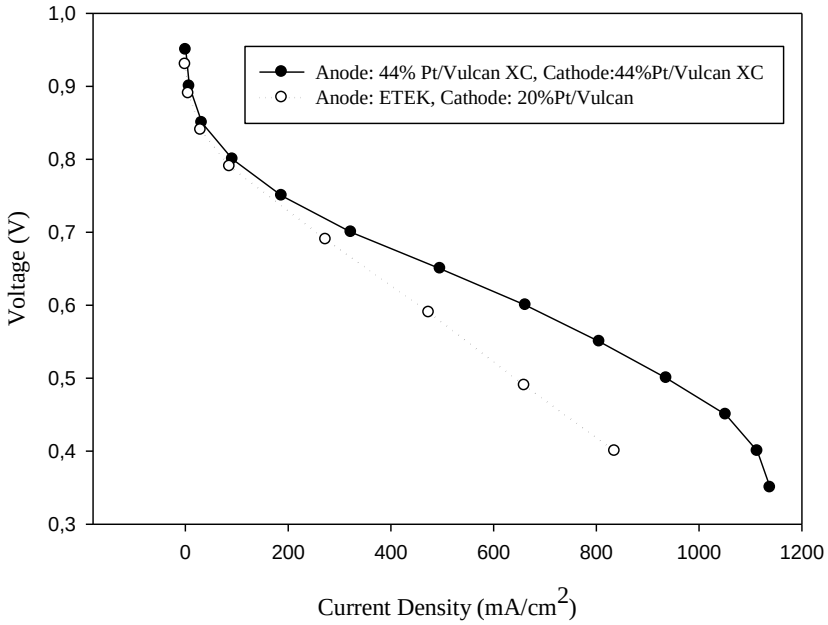

Figure 4.25 PEMFC polarization curve of the Vulcan based catalysts

Figure 4.26 showed the effect of increase in Pt loading on the performance of PEM fuel cell when HCMS carbon support was used as the electrocatalyst support. Two different fuel cells were constructed. One of them was prepared with the 28% Pt/HCMS as both anode and cathode electrocatalysts. Other fuel cell was constructed with commercial 20% Pt/C (ETEK) catalyst as the anode and 20% Pt/HCMS as the cathode. Figure 4.26 also showed that, as indicated in Figure 4.25, increase in the Pt loading has a positive effect on the PEM fuel cell performance. As can be seen from figures that the PEM fuel cell performances were increased as the Pt loading was increased for both Vulcan and HCMS carbon supports.

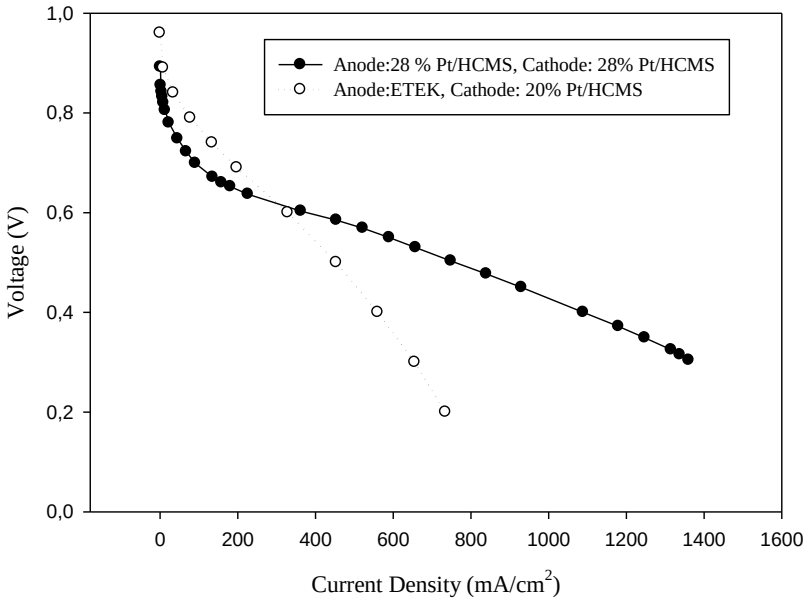

Figure 4.26 PEMFC polarization curve of the HCMS based catalysts

CHAPTER 5

CONCLUSIONS AND RECOMMENDATIONS

The aim of this study was to synthesize mesoporous carbon support material named as hollow core mesoporous shell carbon and prepare their corresponding electrocatalysts with impregnating platinum on carbon supports via microwave irradiation method.

Hollow core mesoporous shell (HCMS) carbon supports were synthesized by two different routes which were based on changing precursor type from phenol/paraformaldehyde to AIBN/Divinylbenzene. From the first route, using phenol/paraformaldehyde couples as carbon source, resulting carbon support exhibited 1053 m^2/g BET surface area and 1.046 nm BJH adsorption pore diameter. To increase the pore size of carbon, divinylbenzene was tried by changing synthesis method and it was realized that carbon support materials' pore size increased accordingly. An additional parameter study was conducted by changing molar ratios of DVB/AIBN from 24 to 20 and 26. As a result the highest pore size was achieved by using molar ratio (MR) of 26. Carbon support material's pore size could be increased up to 3.4 nm with BET surface area of 852 m^2/g in case of 26 molar ratio.

A high surface area of the carbon support was important to have high dispersion for high loading Pt/C, and the pore structure also affects the catalyst dispersion because the micropores may cause the loss of the catalyst dispersion. Therefore, carbon supports with high surface area and low volume of micropores are

the best candidates to achieve high dispersion electrocatalysts, especially for high platinum loadings (Hou et al, 2003). In this study, platinum impregnation was conducted by microwave irradiation method with proceeding 800 W power supply for 120 seconds. Firstly, platinum loading reached up to 44 wt % on commercial Vulcan XC 72 by using moderate amount of ethylene glycol as a reducing agent. To increase platinum impregnated amount on HCMS carbon support, the method was further developed by using different reducing agents such as hydrazine, sodium borohydrate in a combination of ethylene glycol. Platinum loading achieved up to 34 wt % on HCMS carbon support by hydrazine utilization. Accordingly, 34 wt %, 31 wt % and 28 wt % Pt/HCMS carbon supported electrodes preparation was conducted. Characterizations of catalysts were performed by ex situ (N_2 adsorption, TGA, SEM, TEM and Cyclic Voltammetry) and in situ (PEMFC tests) analysis.

Electrochemical characterization of prepared electrocatalysts was performed by cyclic voltammetry. At first, pure HCMS 2.3 was examined by cyclic voltametry up to 500 cycles in order to determine the carbon oxidation. By comparing the results of 20 cycle with 500 cycle, carbon oxidation peak got more significant.

Hydrogen oxidation reaction activity of the catalysts having different platinum loadings were examined by performing 500 cycles to each catalysts at 50 mV/s scan rate under nitrogen flow.

Also, to examine the long term stability of the catalysts 1500 cycles were tried and it was observed that electrochemical active surface area of prepared 32 wt % Pt/HCMS catalysts was 3.117 m^2/g and 1.208 m^2/g for 20 cycles and 1500 cycles, respectively. 61% loss from electrochemical active surface area was observed.

In addition, aging was performed to prepared catalysts for the analysis of carbon corrosion and platinum dissolution ranges. After both aging procedures, the performances of the catalyts decreased significantly. According to cyclic voltammetry tests, 28 wt % Pt/HCMS electrocatalyst exhibited the best performance owing to the highest electrochemical active surface area when compared to 17 wt %

and 32 wt % Pt/HCMS catalysts after 500 cycles. Also, 28 wt % Pt/HCMS catalyst showed less performance loss after 500 cycles for the HOR. Thus, 28 wt % Pt/HCMS 2.3 was selected to test in fuel cell environment. PEM fuel cell tests were also performed by using prepared electrocatalysts at both anode and cathode sides and it was observed that the increase in the Pt loading over the carbon support resulted in an increase in the fuel cell performance.

In order to increase the pore size of the HCMS carbon support it is recommended to increase the pore size of silica templates which will provide a better Pt nanoparticle impregnation. For this purposes the following ways can be followed:

- The current reaction medium was basic with a pH of 10, so it is recommended to use an acidic medium for silica synthesis.
- HCMS carbon support synthesis by 2^{nd} route could be performed at lower molar ratios of AIBN/Divinylbenzene.
- An alternative carbon source such as ethylene glycol, styrene could be tried instead of divinylbenzene.

The Pt loading over the carbon support was strongly affected by the catalyst preparation conditions especially including the type of the reducing agent. By optimizing the ratios of $NaBH_4$ and hydrazine to ethylene glycol, Pt loading over the carbon support can be increased further. Microwave power and duration also can be optimized in order to prepare the catalysts having better properties. To verify platinum agglomeration, it is recommended to characterize the catalyst after degradation tests by TEM analysis.

REFERENCES

Akay, R. G. *Development and characterization of composite proton exchange membranes for fuel cell application*, PhD Thesis, METU, Ankara, 2008.

Andujar, J.M., Segura, F., Fuel Cells: History and updating. A walk along two centuries, *Renewable and Sustainable Energy Reviews* 13 (2009), pp. 2309-2322.

Antolini, E., Carbon Supports for Low Temperature Fuel Cell Catalysts, Review, *Applied Catalysis B: Environmental*, Volume 88, Issues 1-2, 29 April 2009, Pages 1-24.

Barbir, F., *Handbook of Fuel Cell Technology-Fundamentals, Technology and Applications* (Vol. 4), (W. Vielstich, A. Lamm, & H. Gasteiger, Eds.) New York: J.Wiley, 2003.

Barbir, F., *PEM Fuel Cells: Theory and Practice*, Elsevier Academic Press: USA, 2005.

Bayrakçeken, A., *Platinum and Platinum-Ruthenium Based Catalysts on Various carbon Supports Prepared by Different Methods for PEM Fuel Cell Applications*, PhD Thesis, METU, Ankara, 2008.

Bayrakçeken, A., Erkan, S., Türker, L., & Eroğlu, İ., Effects of membrane electrode assembly components on proton exchange membrane fuel cell performance, *Int J Hydrogen Energy* (2008), pp. 165–170.

Bernay, C., Marchand, M., Cassir, M., Prospects of different fuel cell technologies for vehicle applications, *Journal of Power Sources* 108 (2002), pp. 139-152.

Bock, C., Paquet, C., Couillard, M., Botton, G. A., MacDougall, B. R., Size-Selected Synthesis of PtRu Nano-Catalysts: Reaction and Size Control Mechanism, *Journal of American Chemical Society*, 2004, 126, pp. 8028-8037.

Büchel, G., Unger., K. K., Matsumoto, A., Tsutsumi, K., A Novel Pathway for Synthesis of Submicrometer-Size Solid Core/Mesoporous Shell Silica Spheres, *Advance Materials*, 10, (1998), No. 13.

Chai, G. S., Yoon, S. B., Kim, J. H., Yu, J. –S., Spherical carbon capsules with hollow macroporous core and mesoporous shell structures as a highly efficient catalyst support in the direct methanol fuel cell, *Chemical Communications*, (2004), pp. 2766–2767.

Chen, G., Zhang, H., Ma, H., Zhong, H., Electrochemical durability of gas diffusion layer under simulated proton exchange membrane fuel cell conditions, *Int. J. Hydrogen Energ.* 34 (19) (2009), pp. 8185-8192.

Chen, S., Gasteiger, H. A., Hayakawa, K., Tada, T., Shao-Horn, Y., Platinum-Alloy cathode catalyst degradation in Proton Exchange Membrane Fuel Cells: Nanometer-Scale compositional and morphological changes, *Journal of The Electrochemical Society* 157 (1) (2010), pp. A82-A97.

Chung, C. G., Kim, L., Sung, Y. W., Lee, J., Chung, J. S., Degradation mechanism of electrocatalyst during long-term operation of PEMFC, *Int. J. Hydrogen Energ.* 34 (21) (2009), pp. 8974-8981.

Donohue, M.D., Aranovich, G.L., Classification of Gibbs adsorption isotherms, *Advances in Colloid and Interface Science* 76-77, (1998), pp. 137-152.

Ediger, V., *Osmanlı'da Neft ve Petrol*, METU Publications, 3rd Edition, Ankara, 2003.

Ergün, D., *High Temperature Proton Exchange Membrane Fuel Cells*, M.Sc Thesis, METU, Ankara, 2009.

Erkan S., *Synthesis of some metalophythalocyanines and their effects on the performance of PEM fuel cells*, Ms Thesis, METU, Ankara, 2005.

Fang, B., Chaudhari, N., K., Kim, M-S., Kim, J., H., Yu, J-S., Homogeneous Deposition of Platinum Nanoparticles on Carbon Black for Proton Exchange Membrane Fuel Cell, *Journal of American Chemical Society* 131, (2009), pp. 15330–15338.

Fang, B., Kim, J. H., Lee, C., Yu, J.-S., Hollow Macroporous Core/Mesoporous Shell Carbon with a Tailored Structure as a Cathode

Electrocatalyst Support for Proton Exchange Membrane Fuel Cells, *Journal of Physical Chemistry* 112, (2008), pp. 639-645.

Fang, B., Kim, M., Kim, J. H., Yu, J. S., Controllable Synthesis of Hierarchical Nanostructured Hollow Core/Mesopore Shell Carbon for Electrochemical Hydrogen Storage, *Langmuir* 24 (2008), pp. 12068-12072.

Fang, B., Kim, M., Yu, J. S., Hollow Core/Mesoporous Shell Carbon as a Highly Efficient Catalyst Support in Direct Formic Acid Fuel Cell, *Applied Catalysis B: Environmental* 84 (2008), pp. 100-105.

Fıçıcılar, B., Bayrakçeken, A., Eroğlu, İ., Effect of Pd loading in Pd-Pt bimetallic catalysts doped into hollow core mesoporous shell carbon on performance of proton exchange membrane fuel cells, *Journal of Power Sources* 193 (2009), pp. 17-23.

Fıçıcılar, B., Bayrakçeken, A., Eroğlu, İ., Pt incorporated hollow core mesoporous shell carbon nanocomposite catalyst for proton exchange membrane fuel cells, *International Journal of Hydrogen Energy* (2009), doi:10.1016/j.ijhydene.2009.11.016.

Grigoriev, S. A., Millet, P., Fateev, V. N., Evaluation of carbon-supported Pt and Pd nanoparticles for the hydrogen evolution reaction in PEM water electrolysers, *Journal of Power Sources* 177 (2008), pp. 281–285.

Haile, S.M., *Fuel Cell Materials and Components*, *Acta Materialia* 51 (2003), pp. 5981-6000.

Hou, Z., Yi, B., Zhang, H., Preparing High Loading Pt/C by Modifying the Carbon Support, *Electrochemical and Solid-State Letters*, 6, 11 (2003), pp. A232-A235.

Jong-Sung Yu, Suk Bon Yoon, Kwonnam Sohn, Jeong Yeon Kim, Taeghwan Hyeon, Nanostructured Carbon Capsules with Hollow Core/Mesoporous Shell Structure, *International Journal of Nanotechnology* Vol. 3, No.2/3 (2006), pp. 253 – 279.

Kerner, R., Palchik, O., Gedanken, A., Sonochemical and Microwave-Assisted Preparations of PbTe and PbSe. A Comparative Study, *Chem. Mater.* (2001), 13, pp. 1413-1419.

Kim, J.H., Fang, B., Yoon, S. B., Yu, J. -S., Hollow core/mesoporous shell carbon capsule as an unique cathode catalyst support in direct methanol fuel cell, *Applied Catalysis B: Environmental* 88 (2009), pp. 368–375.

Kim, J. Y., Yoon, S. B., Kooli, F., Yu, J. –S., Synthesis of highly ordered mesoporous polymer networks, *Journal of Materials Chemistry* 11 (2001), pp. 2912–2914.

Kim, M., Yoon, S.B., Sohn, K., Kim, C. –H. Shin, Hyeon, T., Yu, J.-S, Synthesis and characterization of spherical carbon and polymer capsules with hollow macroporous core and mesoporous shell structures, *Microporous Mesoporous Materials* 63 (2003), pp. 1-9.

Kim, P., Joo, J., B., Kim, W., Kim, J., Song, I., K., Yi, J., $NaBH_4$-assisted ethylene glycol reduction for preparation of carbon-supported Pt catalyst for methanol electro-oxidation, *Journal of Power Sources* 160 , (2006), pp. 987–990.

Komarneni, S., Dongsheng, B., Newalkar, L., Katsuki, H., Bhalla, A., S., Microwave-Polyol Process for Pt and Ag Nanoparticles, *Langmuir*, 18 (2002), pp. 5959-5962.

LaConti, A., & Hamdan, M. M., *Handbook of fuel Cells: Fundamentals, Technology, and Applications* (Vol. 3). England: John Wiley and Sons, 2003.

Larmini, J., Dicks, A., *Fuel Cell Systems Explained*, Wiley, 2nd Edition, 2003

Lee, J., Kim, J, Hyeon, K., Synthesis of new nanostructured carbon materials using silica nanostructured templates, *International Journal of Nanotechnology* Vol. 3, No.2/3, (2006), pp. 253-279.

Lee, J., Kim, J, Hyeon, T., Recent Progress in the Synthesis of Porous Carbon Materials, *Advance Materials*, 18, (2006), 2073–2094.

Li, J. K., Han, S. Y., Park, S. –K., Park, Y. –K., Lee, C. W., Activation of Nano-sized Carbon Shells on Carbon Hollow Spheres under Water Vapor, *Korean Journal of Chemical Eng*ineering, 22(1), (2005), pp. 42-45.

Lee K., Zhang J., Wang H., Wilkinson D., Progress in the synthesis of carbon nanotube- and nanofiber-supported Pt electrocatalysts for PEM fuel cell catalysis, Journal of Applied Electrochemistry, 36, (2006), pp. 507-522.

Li, X., *Principles of Fuel Cells*, New York: Taylor & Francis Group, 2006.

Maass, S., Finsterwalder, F., Frank, G., Hartmann, R., Merten, C., Carbon support oxidation in PEM fuel cell cathodes, *Journal of Power Sources*, 176 (2008) 444-451.

Marban, G., Solis, T., V., Towards the hydrogen economy?, *International Journal of Hydrogen Energy* 32 (2007), pp. 1625-1637.

Merzougui, B., Swathirajan, S., Rotating Disk Electrode Investigations of Fuel Cell Catalyst Degradation Due to Potential Cycling in Acid Electrolyte, *Journal of The Electrochemical Society*, 153 (12), (2006), pp. A2220-A2226.

Panić, V. V., Stevanović, R. M., Jovanocić, V. M., Dekanski, A. B., Electrochemical and capacitive properties of thin-layer carbon black electrodes, *Journal of Power Sources*, 181 (2008) 186-192.

Rouquerol,F. Rouquerol,J., Sing,K., Adsorption by Powders and Porous Solids, Principles, Methodolog and Applications, *San Diego:Academic Press*, (1999).

Seo, D., Lee, J., Park, S., Rhee, J., Choi, S. W., Shul, Y. G., Investigation of MEA degradation in PEM fuel cell by on/off cyclic operation under different humid conditions, *In press*, doi:10.1016/j.ijhydene.2010.02.053.

Shao, Y., Yin, G., Gao, Y., Understanding and approaches for the durability issues of Pt-based catalysts for PEM fuel cell, *Journal of Power Sources* 171 (2007), pp. 558–566.

Søgaard, M., Odgaard, M., Skou, E. M., An improved method for the determination of the electrochemical active area of porous composite platinum electrodes, *Solid State Ionics* 145 (2001), pp. 31–35.

Song, S., Wang, Y., Shen, P. K., Pulse-microwave assisted polyol synthesis of highly dispersed high loading Pt/C electrocatalyst for oxygen reduction reaction, *Journal of Power Sources* 170 (2007), pp. 46-49.

Staffell, I., Green, R., Kendall, K., Cost targets for domestic fuel cell CHP, *Journal of Power Sources* 181 (2008), pp. 339-349.

Sperling, D., Cannon, J. S., *The Hydrogen Energy Transition: Cutting Carbon from Transportation*, Elsevier Academic Press: USA, 2004.

Stevens, D. A., Dahn, J. R., Electrochemical Characterization of the Active Surface in Carbon-Supported Platinum Electrocatalysts for PEM Fuel Cells, *Journal of The Electrochemical Society*, 150 (6), (2003), pp. A770-A775.

US Patent #7,157,402 B2

Van Blaaderen, A., Van Geest, J., Vrij, A., Monodisperse Colloidal Silica Spheres from Tetraalkoxysilanes: Particle Formation and Growth Mechanism, Journal of Colioid and Interface Science, *Journal of Colioid and Interface Science* Vol.154, No.2, (1992), pp. 481-501.

Vazquez-Huerta, G., Ramos-Sanchez, G., Rodriguez-Castellanos, A., Meza-Calderon, D., Antano-Lopez, R., Solorza-Feria, O., Electrochemical analysis of the kinetics and mechanism of the oxygen reduction reaction on Au nanoparticles, *Journal of Electroanalytical Chemistry* 645 (2010), pp. 35–40.

Von, M.R., Spakovsky, B. Olsommer, Fuel cell systems and system modeling and analysis perspectives for fuel cell development, *Energy Conversion and Management* 43, (2002), pp. 1249-1257.

Wang, B., Recent development of non-platinum catalyst for oxygen reduction reaction, *Journal of Power Sources*, 152 (2), (2005), pp. 1-15.

Wang, J., Yin, G., Shao, Y., Zhang, S., Wang, Z., Gao, Y., Effect of carbon black support corrosion on the durability of Pt/C catalyst, *Journal of Power Sources* 171, (2007), pp. 331-339.

Watt-Smith, M. J., Friedrich, J. M., Rigby, S. P., Ralph, T. R., Walsh, F. C., Determination of the electrochemically active surface area of Pt/C PEM fuel cell electrodes using different adsorbates, *J. Phys. D: Appl. Phys.* 41, (2008), pp. 174004 (8pp).

Xing, W., Qiao, S.,Z.,Ding, R.,G., Li, F., Lu, G.,Q., Yan, Z.,F., Cheng, H.,M., Superior electric double layer capacitors using ordered mesoporous carbons, *Carbon 44* (2006), pp. 216–224.

Yoon, S.B., Sohn, K., Kim, J.Y., Shin, C.-H., Yu, J.,-S., Hyeon, T., Fabrication of Carbon Capsules with Hollow Macroporous Core/Mesoporous Shell Structures, *Advance Material* 14, (2002), pp. 19-21.

Yu, J.–S., Fabrication of Bimodal Porous Silica with Zeolite Crystal Core/Mesoporous Shell and Corresponding Nonspherical Hollow Carbon Capsules, *Rev. Adv. Mater. Sci.* 10, (2005), pp. 341-346.

Yu, J.-S., Yoon, S. B., Sohn, K., Kim, J.,Y., Hyeon, T., Nanostructured Carbon Capsules With Hollow Core/Mesoporous Shell Structure, *Materials Research Society* Symp. Proc. Vol. 728, (2002).

Zaragoza -Martin, F., Sopena-Escario, D., Morallon, E., Salinas-Martinez de Lecea, C., Pt/carbon nanofibers electrocatalysts for fuel cells Effect of the support oxidizing treatment, *Journal of Power Sources* 171, (2007), pp. 302–309.

Zhang,J., *PEM Fuel Cell Electrocatalysts and Catalyst Layers: Fundamentals and Applications*, Springer, (2008).

Zhang, S., Yuan, X., Wang, H., Mérida, W., Zhu, H., Shen, J., Wu, S., Zhang, J., A review of accelerated stress tests of MEA durability in PEM fuel cells, *Int. J. Hydrogen Energ.* 34, (2009), pp. 388-404.

Zhou, S. Y., Li, X. H., Wang, Z. X., Guo, H. J., Peng, W. J., Effect of activated carbon and electrolyte on properties of supercapacitor, *Transactions of Nonferrous Metals Society of China*, 17 (2007) 1328-1333.

APPENDIX A

MEA PREPARATION PROTOCOL

1. Nafion 112 is cut into 5cm*5cm dimensions.

2. GDL 31BC type gas diffusion layer is cut into 2.1cm*2.1 cm dimensions and weighed with a balance (X=tare of the GDL).

3. Catalyst solution is prepared. The amounts of the chemicals given below are based on 20% Pt/C catalyst and 0.4 mgPt/cm^2 on the electrode.

Pt/C amount=(0.4 mgPt/cm2)*(5 cm2)(100 mgPt/C/20mgPt)/1000 =0.01 g Pt/C

Nafion amount=(0.01)*(0.3)/(0.7)=0.0043 g Nafion

Nafion solution amount=(0.0043)*100/5=0.0857 g Nafion solution

3 times more than required amounts per 1 electrode to compensate the losses arised from spraying;

0.03 g Pt/C (20%)

0.2571 g Nafion solution (5%)

2 ml H_2O

4 ml 2 propanol

This chemicals are mixed and then ultrasonicated for 30 minutes and further mixed by homogenizer. Then sprayed onto the GDL by using spray gun and dried by a hot air gun which is set to 80°C.

4. After spraying and drying, the GDL weighed periodically to see if the weight of the GDL is reached to: Xfinal=X+(0.01)+(0.0043) g. If the weight is reached to X final then the GDLs are ready for hot pressing.

5. Two electrodes are prepared in the same way and then they placed on two sides of the Nafion 112 membrane reciprocally. Then the MEA is hot pressed at 130ºC and 250 psi.

6. After the hot press waited for a while for the MEA to cool down and then it is ready for use in fuel cell.

APPENDIX B

SAMPLE CALCULATION

Mass Balance Calculation for SCMS silica formation procedure:

- Addition of 3.14 mL of aqueous ammonia [$NH_{3(aq)}$ (32 wt%)]
  Density of aqueous ammonia = 226.3 g/L

  $m_{aqueous\ ammonia}$ = 226.3 g/L x 3.14 mL x 1L/1000mL

  = 0.71 g

- Addition of 74 mL of ethanol
  Density of ethanol = 0.789 g/mL

  $m_{ethanol}$ = 0.789 g/mL x 74 mL

  = 58.39 g

- Addition of 6 mL of Tetraethoxysilane (TEOS)
  Density of TEOS = 0.98 g/mL

  $m_{1\text{-}TEOS}$ = 0.98 g/mL x 6mL

  = 5.88 g

- Addition of 10 ml of deionized water
  Density of water = 1.0 g/mL

  m_{water} = 10 g

- Addition of 5 mL of TEOS and 2 mL Octadecyltrimethoxysilane (C18TMS)
  Density of C18TMS = 0.883 g/mL

  m_{C18TMS} = 0.883 g/mL x 2 mL

  = 1.77 g

  $m_{2\text{-}TEOS}$ = 0.98 g/mL x 5mL

  = 4.9 g

SCMS- Silica material formation weight before centrifugation assuming that ammonia is not lost.

$$m_1 = m_{aqueous\ ammonia} + m_{ethanol} + m_{1\text{-}TEOS} + m_{water} + m_{C18TMS} + m_{2\text{-}TEOS}$$
$$= 0.71 + 58.39 + 5.88 + 10 + 1.77 + 4.9$$
$$= 81.65\ g$$

After centrifugation and drying processes, it is assumed that ethanol, water and ammonia are removed from the content.

$$m_2 = m_{1\text{-}TEOS} + m_{C18TMS} + m_{2\text{-}TEOS}$$
$$= 5.88 + 1.77 + 4.9$$
$$= 12.55\ g$$

However, the weight obtained after the synthesis was approximately 4.5 g. This means that some chemicals were lost during the centrifugation and drying processes. At the end of the calcination process the weight of the sample was reduced to a value of approximately 3.5 g due to the organic group separation from the content.

Mass Balance Calculation for HCMS carbon support formation procedure:

Basis : 1 gram of SCMS silica template

- 1 g SCMS silica
- Addition of 0.27 g of $AlCl_3.6H_2O$ in 0.3 mL

  $m_{AlCl3} = 0.27$

  $m_{water} = 0.3$ g

After drying process in vacuum oven, it can be assumed that 0.3 mL water is vaporized.

- Addition of 0.374 g phenol
- Addition of 0.238 g paraformaldeyhde

HCMS- carbon material formation weight before centrifuge assuming ammonia is not lost.

$$m_1 = m_{silica} + m_{AlCl3} + m_{phenol} + m_{paraformaldeyhde}$$

$$= 1 + 0.27 + 0.374 + 0.238$$

$$= 1.882 \text{ g}$$

After calcination and etching processes some impurities and silica templates removed from the content. Finally, at the end of the drying process approximetly 1 g of HCMS carbon support can be synthesized.